A MODEL FOR EVALUATING CONTROL

OF UNSTEADY LEADING EDGE

VORTEX FLOWS

By

STEVEN DWIGHT ROBERTS

Bachelor of Science

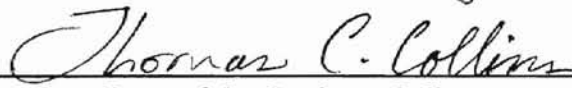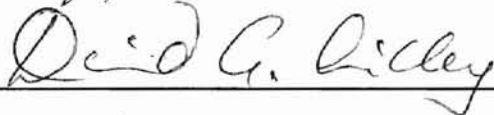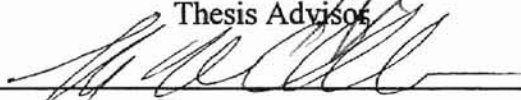Oklahoma State University

Stillwater, Oklahoma

1992

Submitted to the Faculty of the
Graduate College of the
Oklahoma State University
in partial fulfillment of
the requirements for
the Degree of
MASTER OF SCIENCE
July, 1997

# A MODEL FOR EVALUATING CONTROL

# OF UNSTEADY LEADING EDGE

# VORTEX FLOWS

Thesis Approved:

_____

Thesis Advisor

_____

_____

David G. Lilley

_____

Thomas C. Collins

Dean of the Graduate College

# PREFACE

This study was conducted to provide new knowledge and tools for investigating control of unsteady leading edge vortex flows typically found on highly swept aircraft planforms. Methods for controlling the unsteady strength and spatial characteristics of the vortices in the flowfield using leading edge flaps were modeled and compared to existing experimental data. The model has also provided a method for investigating new ideas in control of unsteady separated vortical flows.

TABLE OF CONTENTS

# LIST OF FIGURES

# NOMENCLATURE

$C_l$ $\equiv$ roll moment
$C_l'$ $\equiv$ sectional roll moment
CFD $\equiv$ computational fluid dynamics
$C_p$ $\equiv$ coefficient of pressure
$c_r$ $\equiv$ root chord length
$I_x$ $\equiv$ inertia in roll of the delta wing
$K$ $\equiv$ feedback gain constant
$L_{aero}$ $\equiv$ total roll moment due to aerodynamic effects
$m$ $\equiv$ total number of panels
$\mathbf{q}$ $\equiv$ velocity vector
$\mathbf{q}_{body}$ $\equiv$ velocity vector of the body
$\mathbf{q}_\infty$ $\equiv$ freestream velocity vector
$t$ $\equiv$ time
$t^*$ $\equiv$ non-dimensional time $= tV_\infty/c_r$
$u_p$ $\equiv$ local velocity on a panel in the x direction
$u_v$ $\equiv$ local velocity on a panel in the x
         direction due to a vortex
$V_n$ $\equiv$ velocity of the body normal to the panel in
         local coordinates
$w_p$ $\equiv$ local velocity on a panel in the z direction
$w_v$ $\equiv$ local velocity on a panel in the z direction
         due to a vortex
$\alpha$ $\equiv$ angle of attack
$\delta$ $\equiv$ flap angle
$\Gamma_l$ $\equiv$ total vorticity of the left primary vortex
$\Gamma_r$ $\equiv$ total vorticity of the right primary vortex
$\Lambda$ $\equiv$ sweep angle
$\gamma$ $\equiv$ vortex strength / panel length
$\Phi$ $\equiv$ flowfield potential
$\phi$ $\equiv$ roll angle
$\dot{\phi}$ $\equiv$ roll rate
$\ddot{\phi}$ $\equiv$ roll acceleration
$\sigma$ $\equiv$ source strength / panel length

# CHAPTER 1

## INTRODUCTION

### 1.1 What performance criteria has dictated the use of separated vortical flows?

In attempting to control unsteady leading edge vortex flows, it is important to understand which performance criteria have driven the design of the vortex flows. Ever since the first flight at Kitty Hawk, aircraft designers have been striving to expand the flight envelope and performance of aircraft. Performance advances such as higher cruise velocities and greater maneuverability have been gained, but not always without expense.

### 1.1.1 Higher velocities

Many designs have attained higher cruise velocities by sacrificing aerodynamic efficiency. The inefficiencies are reflected largely in drag penalties and thus the fuel economy of an aircraft.

#### 1.1.1.1 Examples

The associated trade-offs may have been acceptable when the technology was first demonstrated in aircraft such as the McDonnell F-101 Voodoo, General Dynamic F-102 Delta Dagger, or the Convair B-58 Hustler; however, the inefficiency of these technologies is no longer acceptable. For example, one of the main design criteria of

1

Lockheed Martin's F22 aircraft is supercruise, the ability to achieve supersonic flight without the aid of an afterburner.

## 1.1.1.2 Consequences of higher velocity with more efficiency

Aircraft designers today rely heavily on swept and delta wing geometries to maintain aerodynamic efficiency for a number of reasons. The benefits of swept wing geometries discovered in 1935 by Busemann, Betz, and Prandtl are lower wave drag at supersonic cruise speeds. Building on their efforts, they later show that swept wing and delta wings designs keep the local chord-wise flow subsonic. By maintaining locally subsonic flow, swept wings also experience a smoother increase in drag in the transonic region. The overall benefit of using swept and delta wings was in alleviating shock wave inefficiencies in the transonic and supersonic regions.

These designs, while solving some of the difficult aspects of high subsonic and supersonic flight, create other problems. While a design can be optimized for cruise performance, often the lift to drag performance at lower subsonic speeds is poor due to swept wings having lower aspect ratios. The effect of a lower aspect ratio is to increase induced drag. Therefore, lower lift to drag ratios require higher landing velocities to maintain control of the aircraft.

## 1.1.2 Controllability / Maneuverability

## 1.1.2.1 Landing regime

At the lower speeds maneuverability and controllability issues become even more important, especially when lower speeds are associated often with proximity to the ground

as in the taking off and landing phases of flight. These designs create other problems also. In the case of swept and delta wings, the same design criteria which lead to more efficient cruise performance often diminishes safety for two reasons. First, swept wing planforms can generate unrecognized aerodynamic characteristics which result in controllability and safety problems in "off-design" regions. Secondly, because of having been optimized for cruise performance, the lift to drag performance at lower subsonic speeds is poor due to swept wings having lower aspect ratios. For a constant aircraft weight, lower lift to drag ratios require either higher landing velocities to maintain lift and/or higher angles of attack to control the aircraft.

### 1.1.2.1.1 Consequences

So far, designs fulfilling each one of these criteria have disadvantages. Both result in higher landing speeds that can result in crashes with higher kinetic energy increasing the chance for loss of life and aircraft. Furthermore, high angles of attack have associated controllability problems. Aircraft aerodynamics in lower speed, "off-design", and high angle of attack regimes can be unsteady and result in unsteady vehicle motion.

### 1.1.2.1.2 Examples

This fact is demonstrated by an old phenomenon known as wing rock which is an uncommanded lateral limit cycle oscillation. NASA's High Angle of Attack F-18 research Vehicle (HARV) demonstrated how unsteady aerodynamics at high angles of attack could result in uncommanded roll mode fluctuations. The fluctuations can be limit cycle oscillations as in the case of the NASA's HARV F-18. However, the motion need not be a limit cycle[1]. The unsteady aerodynamics can result in divergent motion as on the

X-31. Even during steady state limit cycle oscillations on the HARV F-18, the amplitude of the motion can be slightly fluctuating about a steady state amplitude.

## 1.1.2.2 Maneuvering

Fighter maneuvers although usually not at lower altitudes do not occur at supersonic cruise velocities. Therefore, lift performance suffers for the same reason as in landing phases of flight. A smaller aspect ratio creates less lift for a given angle of attack; rate of climb diminishes as a result. Maneuvering problems where the ability to track an adversary is important are more difficult. The maneuvering envelope in many cases is diminished to remove the possibility of uncommanded vehicle motion.

At the very least, controllability problems during landing phases along with maneuverability or tracking problems during flight increase the work load on the pilot if the maneuvering envelope is not diminished.

## 1.1.3 Solution in using separated vortical flows

The essential need for safety during take off and landing phases of flight along with the desire for increased maneuverability has demonstrated the benefits of using separated vortical flows. Separated vortical flow improves the L/D ratio at subsonic speeds as well as the maneuverability of the delta wing aircraft at moderate angles of attack. Performance is improved by the vortices over the wing creating additional low pressure regions. As angle of attack increases, the vortices' strength increases providing a decreasing pressure over the wing[49]. The integrated effect being additional lift.

1.2  How are separated vortical flows generated?

Separated flows for the most part are generated using sharp leading edges of wings and smaller secondary vortex generators.  Viscosity causes the freestream flow impinging on the leading edge of the wing or vortex generator to separate.  The shear layer emanating from each sharp leading edge coalesces into a coiled shear layer.  At low to moderate angles of attack these vortices maintain a fairly stable position and strength.  As the angle of attack increases, the strength of the vortices increases also.  However, with the advent of high angle of attack maneuvering,  these same vortices develop a hysteresis in position and strength.

Vortex flow can also be generated using turbulent separation conditions in the boundary layer.  By designing a pressure gradient in the boundary layer inconsistent with turbulent separation the flow can remain attached.  If desired, the flow can be made to separate.

1.3  Why is control of Leading Edge Vortex Flows needed?

The hysteresis in these methods of vorticity generation often pose new problems because the maneuverability of the aircraft is coupled with the unsteady aerodynamics. The problem then becomes one of how to control these separated vortical flows so that the aircraft has desirable handling qualities in all flight modes while increasing the

maneuverability of the aircraft itself. Control of these separated vortical flows will allow the exploitation of lift and moment to increase the maneuverability of the aircraft.

Under certain conditions the hysteresis in the unsteady aerodynamics can lead to erratic motion in roll and yaw of the aircraft. However, aircraft which have highly swept planforms can exhibit a self-induced oscillatory dynamic roll mode of motion known as "wing rock"[49]. Even with a highly swept planform, wing rock is still very dependent upon specific geometric factors. Wing rock is characterized by a buildup to a limit cycle oscillation which is independent of initial conditions.

Control of the separated vortices is fundamental in problems such as wing rock. Vortex control is critical to designs of proposed civilian supersonic aircraft that will operate at high angles of attack during approach and landing to attain a low airspeed. Tactical aircraft which routinely operate at high angles of attack during combat maneuvers are also limited in performance by the onset of wing rock oscillations. In order to expand the operating envelope of these types of aircraft, the problem of dynamically controlling the vorticity distribution through separated vortices must be understood.

1.4 Control methodology of Leading Edge Vortex Flaps

Investigation of all of the many methods that could dynamically control leading vortex flows is nothing short of daunting. The methods available for investigation of vortex flows are the traditional experimental methods along with the computational fluid dynamic (CFD) methods. Both methods yield a great amount of detailed data while requiring a great amount of effort to glean general trends for a wide range of parameters.

Problems arise with studying dynamic problems experimentally with outside factors becoming important. Factors often considered are whether the motion being modeled is the being reproduced accurately. Simplifications to the experimental apparatus may limit investigations to studying one degree of freedom at a time. Then synthesizing the data back to get a feel for how the multiple degree of freedom of problem is behaving is difficult. Experimental methods provide a good feel for the actual situation if an experiment is designed properly.

With the difficulty in obtaining information experimentally, often it is difficult to design an experiment to investigate only the fundamental parameters. The phenomenon being studied may be a function of several parameters of which most cannot be directly measured i.e. the state of the experiment is not completely observable. Add the complexity of measuring an unsteady flowfield and the design of the experiment becomes just as complicated as the phenomenon being researched.

Likewise, computational methods such as Navier Stokes solvers can yield vast amounts of data. Just with even a steady flow solution, questions concerning meshing of the computational domain can impede a general search to validate new concepts. If the flow solution is then coupled with the equations of motion for an aircraft, the amount of data to be understood is overwhelming. Since the boundary conditions are changing in a dynamic solution of a flow field, the meshed domain also changes. Remeshing a computational domain at every time step slows a solution procedure immensely. Predicting any dynamic motion that may be produced by varying the strength and position of vortices is certainly intractable if a wide range of parameters are being investigated using CFD methods. However, once the range of parameters has been narrowed, CFD

methods provide very detailed information applicable to detail design. At the preliminary design, important larger trends can be obscured by the quantity of data.

## 1.5 Basis for Tool

During the preliminary stage of studying the feasibility of several or many promising ideas for controlling leading edge vortical flows, only as much data as needed to distinguish one idea over another is needed. Once a distinction is made between the ideas, the more feasible options can be researched in greater detail. But a full study of each of the preliminary ideas leads to a test matrix size that is intractable at best. By refining the test matrix and studying only the more promising ideas, a solution to a problem can be found and understood sooner. In order to refine a large test matrix, a tool is needed that is much faster than either experimental of computational research efforts are. Distinctions between preliminary ideas are often found in the primary characteristics of the flow field. Therefore, a tool is needed that is flexible enough that it can be used with all of the ideas being studied, faster than traditional methods, but does not necessarily need to be as accurate. These criteria can be accomplished by using simplifications to the flowfield model that will reveal trends in the implementation of the new designs within the specific limitations of the model.

### 1.5.1 Experimental Techniques for Modeling Wing Rock

A new tool certainly could be developed from a simplification of existing techniques or a completely new method could be developed that would meet this criteria. Experimental techniques are difficult to simplify since much of the data acquisition

techniques tend to be very tedious. Also, accurate, detailed models must be constructed for each idea to be studied. Furthermore, measurements of a dynamic flowfield are difficult to obtain due to constraints of the test apparatus, often times. For example, a single laser doppler anemometer cannot measure unsteady vorticity since vorticity must be differentiated from the velocity flow field. Primarily, the desired results from the new tool are a simpler method for reducing the feasibility test matrix.

## 1.5.2  Computational Techniques for Modeling Wing Rock

Computational methods on the other hand are easier to simplify. Assumptions and observations can be made which simplify the basis for the model. The implementation of the model is reduced before a solution is sought. These same assumptions and observations can refine the search for a solution method. Therefore, by using simplifying assumptions in computational methods, a more efficient solution can be realized.

## 1.5.2.1  Navier Stokes and Euler Techniques

Since separated vortical flowfields are being studied, the flowfield is assumed to be inviscid. This eliminates the stress gradient terms from the Navier Stokes equations leaving only the convective acceleration terms along with the time derivative terms. From continuity, the divergence of the velocity field can be rewritten in terms of a potential function if the flowfield is assumed be irrotational. The continuity equation then becomes Laplace's governing equation. If a solution of an unsteady form of Laplace's equation is implemented that is fairly quick, then the requirements for a new tool are met.

Computation techniques in modeling the flow phenomenon of wing rock have been

accomplished by the numerical solution of the Navier Stokes equations, Euler solution techniques, and potential theory. Numerical simulation of unsteady delta wing flows at constant roll rates using Navier Stokes equations have been implemented by Gordnier and Visbal[2]. Chaderjian[3] has used a Navier-Stokes simulation code to obtain data for static and forced dynamic motion cases. These methods are able to match experiment almost exactly, but even on the most advanced computers, these methods are costly in CPU time.

1.5.2.2 Inviscid, Potential Techniques

Potential flow models for steady delta wing flow fields have been used by Brown and Michael[4], Mangler and Smith[5], and Konstadinopoulos, et al.[6] More recently, Arena and Nelson[7] present experimental studies along with computational models that show that the limit cycle oscillation of the wing rock phenomenon can be captured by modeling only the primary physics of the aerodynamic characteristics. Arena's model assumes an inviscid flow field in which all the vorticity is concentrated into two leading edge vortices. The inviscid assumption for unsteady delta wing flows for angles of attack where vortical breakdown is not present has been suggested by Arena and others. Their suggestion is based upon experimental investigation since a large angle of attack region exists where wing rock is present but vortex breakdown is not seen.[8] Also, slender wing theory along with a conical flow field assumption was used to simplify Arena's model to improve computational time. This assumption is based on and justified by experimental results for delta wings with no breakdown present. To use the conical flowfield assumption, the properties of the flowfield must be functions primarily of the lateral and normal coordinates of the wing. This is true for a steady flow field, but the boundary condition for the unsteady motion proves the conical assumption mathematically invalid. The

boundary condition for a rotating wing or normal velocity of the body is not constant along conical rays, but of rays parallel to the axis of rotation. Again, experimental evidence shows that conical flow qualitatively holds for flowfield for the unsteady case; however, the flow is only locally conical in the unsteady case instead of globally conical as in the steady case. A consequence of locally conical flow is that a solution is found for a particular chord station and is then linearly scaled for the other chord stations.

These assumptions allow the three dimensional flow field to be approximated using a two dimensional model. The model qualitatively captured all characteristics observed in experiment including unsteady behavior of $C_l$, vortex position, and $C_p$. Presently, the physics causing wing rock has been obtained so that methods that suppress or exploit the wing rock phenomenon can be developed.

1.6 Rationale for Developing an Inviscid Model

The primary motivation for developing an inviscid model is to systematically investigate a variety of control schemes for controlling unsteady separated leading edge vortical flows on delta wings. In searching for solutions that will allow dynamic control, a great number of possible configurations exist that may by successful. Experimental investigation of all of the many possibilities that exist even with one configuration makes the problem practically intractable. Computational investigation requires a significant investment in computational time. Navier Stokes simulations can take hundreds of hours to obtain a single cycle of motion. To study wing rock suppression, for example, between 50 and 100 cycles would be needed to capture the transient, steady state, and control suppression. This translates into an enormous cost in time with the many trial cases that

need to be investigated to find a solution to wing rock. However, both experimental and CFD investigations yield detailed flow characteristics that certainly could not be captured with an inviscid model alone. The inviscid model developed will augment the number of methods already being used. Inviscid modeling has been proven to capture a variety of unsteady vortical flowfield characteristics while accomplishing the task within a couple of hours on a mid size workstation.[9] Primary investigation with an inviscid model would help in limiting the experimental test matrix size by eliminating the methodologies that do not demonstrate control of unsteady separated vortical flows within the limitations of the model.

CHAPTER 2

LITERATURE SURVEY

2.1 Leading Edge Vortex Flow Control for Wing Rock

Study of leading edge vortex flows started in the 1950's on delta wing planform designs. The advantages of using delta wings to generate leading edge vortex flows are two fold. Highly swept delta wings have favorable drag characteristics for supersonic cruise at low angles of attack. Additionally, the leading edge vortex flows generate higher lift at moderate angles of attack using strong vortices which emanate from the sharp leading edges. A more balanced design can be achieved using delta wings since they have both efficient supersonic cruise with capability to maneuver subsonically at high g loading.[10]

Control can enhance an aircraft's characteristics in the subsonic or supersonic flight regimes. The leading edge vortex flow control can be applied to either supersonic cruise or subsonic maneuverability, and for each of these regimes control can be implemented statically or dynamically. As with many other types of aerodynamic research, understanding control of static phenomenon historically has been pursued first since static data is easier to obtain and is more intuitive. Static results often aid in understanding dynamic phenomenon as well.

Studies in the early 1980's by Herbst[11], Lang and Francis[12], and Ashely[13] showed that a tactical advantage could be gained by exploiting increased subsonic maneuverability

13

in the high angle of attack post stall regimes of delta wings. This review will address only those efforts aimed at increasing subsonic maneuverability either through static or dynamic control of leading edge vortex flows. Several methods have been used recently to investigate controlling separated leading edge vortex flows. These investigations fall into three main categories: a mathematical controls only viewpoint, investigations that use changes in geometry to control the separated leading edge vortical flows, and investigations that manipulate the flowfield by blowing from the boundary layer.

2.1.1 Systems Approach

Hsu and Lan[14] first developed a mathematical model of wing rock in 1985. Their model was developed for one dimensional motion and three dimensional wing rock motion to identify the major parameters involved in wing rock. The model was able to predict wing rock closely using Beecham and Titchner's[15] method to determine the parameters. The assumed mathematical form for wing rock that they used is shown below.

$$\ddot{\phi} = L_0 + \sin\alpha_s L_\beta \phi + L_{p0} \dot{\phi} + \sin\alpha_s L_{p\beta} |\dot{\phi}|\phi + L_{pp}|\dot{\phi}|\dot{\phi}$$

where $\phi$ is the roll angle, and $\alpha_s$ is the steady angle of attack.

Elzebda, Nayfeh and Mook[16,17] compare Hsu and Lan's model and two other derivative models to a slender delta wing mounted on a free-to-roll sting. The derivative models were developed by the authors to study the effect of the assumed nonlinear form of the roll moment with roll angle and its derivative. They show that Hsu and Lan's model cannot predict roll divergence since the original model only contains quadratic terms. With the addition of a cubic term, the model predicts roll divergence and predicts the wing rock motion more closely than the original model. Their second paper presents a

more global view of the wing rock phenomenon. The mathematical model was used to construct phase planes which reveal the characteristics of wing rock such as stable limit cycles, unstable foci, saddle points, and domains of initial conditions leading to oscillatory motion and divergence. The phase planes of roll rate versus roll angle reveal primary characteristics of wing rock and the effects of planform geometry on those characteristics.

Luo and Lan[18] adopt Hsu and Lan's mathematical model for the non-linear wing rock motion. Luo and Lan only study the one dimensional case, however. The main objective of Luo and Lan's effort was to find a control function that would suppress the wing rock motion. In order to do this, an arbitrary control variable, u was added to the equation of motion.

$$\ddot{\phi} = L_0 + \sin\alpha_s L_\beta\,\phi + L_{p0}\dot{\phi} + \sin\alpha_s L_{p\beta}|\phi|\dot{\phi} + L_{pp}|\dot{\phi}|\dot{\phi} + u$$

Again, the resulting governing equation was solved using Beecham-Titchner's averaging technique which splits the solution into a in-phase part for the frequency and an out-of-phase part for the amplitude. The optimal control input to suppress wing rock was determined through a Hamiltonian method. The specific case for an 80 degree delta wing was numerically solved using these methods to show that Beecham-Titchener's technique is accurate in analyzing dynamic motion and determining an optimal control input. For an 80-degree delta wing, the following values for the aerodynamic characteristics were used :

$L_0 = 0.0$

$\sin\alpha_s L_\beta = -26.6667 \; \sec^{-2}$

$L_{p0} = 0.764785 \; \sec^{-1}$

$\sin\alpha_s L_{p\beta} = -2.92173 \; \text{rad-sec}^{-1}$

$$L_{pp} = 0.0$$

The most significant result that Luo and Lan obtained was that it is sufficient to use a linear feedback of state variables, such as roll rate, to suppress wing rock. Also, the system sensitivity to aerodynamic coefficients was determined to be a function of system damping. Higher sensitivity was obtained for a system with lower damping.

2.1.2 Aerodynamic Control

Even though it was determined by Luo and Lan[18] that the optimal control scheme was through the feedback of state variables, how to effectively affect those state variables was not determined. Without understanding the aerodynamic mechanism involved in separated leading edge vortex flows, any method that could influence the state variables would be just as feasible as the next method. The second method controls separated leading edge vortex flows through manipulations of the geometry. The major difference between these methods and the controls only viewpoint is in understanding what is happening aerodynamically. Although the controls viewpoint may actually use flaps or another control device to stabilize the motion just as with the following efforts, the controls viewpoint only use information available about the motion of the instability through state variables. Control through geometric changes makes an effort to understand the aerodynamic cause of the instability. The aerodynamic phenomenon driving the instability is then controlled by altering the flowfield. The flowfield is altered by changing the geometry in some manner which will be described below. These changes to the geometry can be implemented passively or actively through feedback of a property of the flowfield.

The first attempts at improving the capabilities of delta wings by modifying leading edge vortex flows stemmed from the drag penalties associated with vortex lift. When using vortex lift, subsonic maneuvering is potentially constrained by engine thrust or fuel consumption due to drag. An alternative to this problem is to trade vortex lift for potential lift by extending the angle of attack range of potential lift.[19] The range of potential lift is extended by controlling the leading edge vortex flow. Potential flow is achieved by promoting attached flow as long as possible. This is normally achieved through leading edge bluntness. Robins and Carlson[20] report that additional potential flow achieved through leading edge bluntness is not counter productive to supersonic cruise conditions, as it may seem, as long as the flow remains attached and the wings are swept behind the Mach cone. In fact, supersonic cruise is enhanced by recovery of the leading edge suction of potential flow.

The second reason for modifying or controlling leading edge vortex flows results from stability problems in aircraft having swept delta wings. Control of longitudinal stability problems as well as lateral stability problems such as wing rock need to be controlled in order to gain more and more maneuverability.

## 2.1.2.1 Geometric Control through Geometric Modifications

Rao[16] reported in 1981 that for swept wings up to 40 degrees, leading-edge slots and flaps have proven effective. However, during high g subsonic maneuvering, structures which support the flaps are plagued by distortion effects which complicate actuation. For delta wings swept over 40 degrees, Rao explores the use of fences, "pylon" vortex generators, slots, and plates to enhance drag characteristics as well as control stability

problems passively. The four devices represented three fundamentally different approaches: 1) modifications of leading edge upwash to obtain a camber effect with fences and pylon vortex generators, 2) compartmenting the swept leading edge into "two-dimensional" segments using chordwise slots, and 3) forcing separation to produce a leading edge vortex.

Using a 60 degree swept wing with fences, Rao found that optimum position for a fence is located at the 50 % span point. Additional fences were found to be effective in controlling spanwise flow and in promoting flow attachment. This increased the potential lift and decreased drag. Drag reductions up 25% were found when using pylon vortex generators. By delaying separation, these methods delayed the onset of longitudinal instability also.

Slots were found to reduce drag as the other fence methods although the characteristics of the device were different. Dynamic longitudinal instabilities were aggravated, however. Vortex plates were able to reduce drag and alleviate the longitudinal instabilities by introducing a component of thrust along the leading edge of the delta wing.

Marchman[21,22] conducted wind tunnel test to determine the aerodynamic effects of leading edge flaps deflected upward. Marchman used a 60 degree and 75 degree swept wing. Various sizes and shapes of leading edge vortex flaps were used. It was found that inverted vortex flaps created strong lift, but the flaps also created additional drag. Large changes in lift were not accompanied by large changes in pitching moment. With these characteristics, a properly designed negatively deflected flap may be desirable for landing

conditions. Leading edge vortex flaps were also found to be more effective as sweep increases.

Grantz and Marchman[23] study the effect of trailing edge flap deployment on leading edge vortex flap aerodynamics. On the same 60 degree and 75 degree delta wings as above, they establish that trailing edge flaps do not significantly improve the vortex flowfield. Comparisons of computations generated to study effects of yaw and vortex flaps were made by Murman[24] and Powell and Murman[25] in 1986. The computations were generated and validated for the conical Euler Equations in the supersonic flight regime for an ideal flat plate delta wing whose geometries included thickness, sharp leading edges, and two vortex flaps. Murman and Rizzi[26] review the applications of Euler equations to sharp edge delta wings with leading edge vortices. Freestream Mach numbers from zero to supersonic are discussed.

Ng and Malcom[27] investigated how the forebody vortices on a F/A-18 could be controlled. The flowfield of a highly slender forebody at high angle of attack is dominated by vortices which can present stability problems if they become asymmetric. Ng and Malcolm implement a small rotatable strake on the forebody which can be fixed in place or deployed actively. The strakes generate vortices from the leading edge and trailing edge. These new vortices dominate the forebody flowfield and help maintain attached flow on the forebody. More importantly, the flow asymmetries are able to be controlled and exploited. The strakes could generate yawing moments of different magnitude by moving the strakes to different angular positions. This method of controlling separated vortices was shown to be highly effective in controlling the flow on the forebody over a wide range

of angles of attack and sideslip. The strength of the vortices generated by the strake can be manipulated by changing the shape of the trailing edge of the strake.

Synolakis, et al.[28] use extended leading edge winglets to study passively controlling delta wing rock. The winglets are flaps which linearly increase in chord on the leading edge of the wing. Other authors such as Klute[31] have termed similar types of flaps as apex flaps. The basis for using the winglets is to interfere with the formation of the primary vortices emanating from the leading edge. They summarize that the critical angle at which the onset of wing rock occurs is highly dependent upon the particular geometric configuration. Delta wing geometries with winglets behave much like the baseline delta wing except that the onset is delayed. Extended winglets with a winglet-length to chord-length ratio of 0.43 appear to increase the wing rock envelope the most. Based on their result for an 80 degree delta wing, the angles of attack where the onset of wing rock occurs can be delayed by as much as 25 degrees for moderate angles of attack. By delaying the onset, passive control can be an effective method for improving the stability of the delta wing by expanding performance envelope. No flow visualization was done to confirm the objective of interfering with the formation of the primary vortex structure.

Walton and Katz[29] used control flaps on the leading edges of a one-degree-of freedom in roll model. By driving the flaps out of phase with the roll angle, wing rock was suppressed. The amplitudes of the flap oscillations were such that primary vortices were modified just enough to suppress wing rock. Walton and Katz state that the flaps in their investigation would be more effective if the leading edge of the wing was thinner. Also, the flaps would be more effective if the placement of the flaps was farther forward. This indicates that the control mechanism used modifies the characteristics of the

separation and the roll-up. They conclude that the same method theoretically could be implemented along with an active control scheme to suppress wing rock on an actual aircraft configuration.

For a delta wing in a slight side slip, Ng, Skaff, and Kountz[30] developed a methodology using flow dividers on the top of the wing to control wing rock. Flow dividers are vertical fences mounted on the upper side of the wing. The fences or dividers attempt to decouple the flow of each side from the other side's effects. Their results provide an interesting insight into the phenomenon of wing rock itself. By decoupling the flowfield, it was hypothesized that roll oscillations would diminish. Ng, et al. investigated the effects of divider geometry, sizes, and placement and the effect upon the roll oscillations. They were able the suppress wing rock for a wide range of angle of attack; however, at the lower range of $\alpha$'s where wing rock first occurs, the divider actually amplified wing rock. As expected, the divider decreased the roll moment for moderate angles of attack, damping the wing rock oscillation. Also, for angles of attack where the divider amplifies the wing rock oscillation, the divider increased the roll moment at a side slip condition. The divider was able to damp the wing rock motion because it decreased the vortical interactions taking place in the flow field. Also, damping occurred at higher angles of attack where vortex breakdown was present partly because the breakdown is asymmetric and out of phase with roll rate. The asymmetry in the position of the vortices is due to the vortices dependence upon the flow conditions at separation.

Klute, et al.[31] performed an experimental study on controlling vortex breakdown on delta wings. Several control surfaces were tested in fixed and dynamically pitching delta wings. Klute used flow visualizations, surface pressure measurements and Laser-

Doppler Velocimetry measurements to map the flowfield. Vortex breakdown was delayed by implementing a drooping apex flap or "winglet". An apex flap is a leading edge flap whose chord increases linearly. An apex flap typically has a chord which is a set percentage of the local semi span of the wing. Delays by as much as 8 degrees past the steady state angle of attack for breakdown were achieved.

Syverud, et al.[32] implemented an 80 degree leading edge extension as a vortex flap on a 70 degree delta wing. The results obtained were based on qualitative flow visualization studies performed in the 16 x 24 inch water tunnel at NASA - Langley. The leading edge extension is body hinged and serves to control the roll oscillations . The joint between the trailing edge of the leading edge extension and the leading edge of the main wing is swept forward. Dihedral leading edge extension deflection was found to stabilize the primary vortex system while it was found that an anhedral deflection destabilized the vortex system. Once destabilized, the vortex system exhibited rapid vortex breakdown. The delta wing has three vortex structures which dominate the flowfield: the leading edge extension vortex, inboard wing vortex, and outboard wing vortex. With no deflection of the leading edge extension (LEX), the flowfield is similar to delta wing flowfields reported by other investigators. As angle of attack is increased vortex breakdown advances upstream, and it appears on top of the wing at the trailing edge at an angle of attack of 33 degrees. With no LEX deflection, no inboard wing vortex is present. As the LEX is deflected upward, the flowfield stabilizes. The upward deflection strengthens the outboard vortex by displacing the wake disturbance from the LEX. Downward deflection of the LEX causes breakdown of LEX vortices to move farther up on the wing while preventing the outboard vortices from forming. Vortex positions change with LEX

deflections also. As an upward or dihedral deflection increases, the LEX vortex is bent outboard and closer to the wing by the outboard vortex. The bevel of the leading edges and trailing edges of the delta wing were found to destabilize the vortex system if the bevels were on the upper surface of the wing. The upward facing bevels also bend the LEX vortices outboard.

Rinoie and Stollery[33] investigated the use of vortex flaps and vortex plates on delta wings as a means to improve the lift/drag ratio. Force measurements were obtained along with surface pressure measurements in a low speed wind tunnel for a 1.15m span, 60 degree delta wing. The tunnel speed was set at 30 m/s. Results for the vortex flap showed that the lift/drag ratio improved with the deflection of the vortex flap. The improvement was attributed to the flow either not separating at the leading edge of the vortex or the flow reattaching to the flap after separating. The normally large separated zone would be small and enclosed. By keeping the flow attached, the lift increased. The tests were performed by deflecting the flap from 0 to 60 degrees as angle of attack is swept from -8 to 57 degrees. The results for a flap deflection of 30 degrees are presented due to the 30 degree deflection showing the best performance over a wide $C_L$ range. They demonstrate that as far as improving the lift/drag ratio is concerned no improvement is seen once the flow is completely separated at angle of attack of about 35 degrees. Before 30 degrees angle of attack, the greatest improvement in L/D ratio for a leading edge vortex flap deflection of 30 degrees is 40% at a $C_L$ of 0.45. All pressure measurements were performed at $x/c_r = 0.4$ and $x/c_r = 0.8$. By using the pressure measurement data, the effect of the vortex flaps on the pitching moment, $C_m$, is little if not at all.

The spanwise pressure distribution reflected the reattachment of the flow at low angles of attack up to about 6 degrees for no flap deflection. A definite formation of the primary vortex structure typically found on delta wings occurs between $\alpha = 12.4$ and $37.0$ degrees. By $\alpha = 37$ degrees, the pressure distribution spreads out signifying the arrival of vortex breakdown on the upper wing surface. The vortex flow completely collapses at $\alpha = 48.7$ degrees as demonstrated by the pressure distribution being flat. Much the same steady results are obtained for the 30 degree flap deflection case except that the flow remains attached until about an angle of attack of 12 degrees. So, vortex flaps are able to increase the L/D ratio by increasing lift and by reducing drag by reattaching the flow at lower angles of attack. The shape of the low pressure peaks due to the primary vortex structure is slightly different between the two flap setting suggesting the location and/or strength changes with the flap setting. This is plausible since the vortex flap is able to reattach flow at lower angles of attack. Rionoie and Stollery[33] present pressure distribution results at $x/c_r=0.4$ where the flap angle is swept from 0 to 60 degrees while angle of attack is held constant at 6 and 12 degrees. At an angle of attack of 12 degrees for flap angles up to 30 degrees the primary vortices move outboard as the flap angle increases. As the flap angle is increased past 30 degrees the separation at the leading edge of the flap attaches and a line of separation forms just inside of the hinge line.

The effect of vortex plates are also investigated for improving the L/D ratio. As implemented in their study, a vortex plate is a thin plate fastened to the lower side of the leading edge. The plate serves to extend the separation point out from the actual wing's leading edge. The vortex plates were able to obtain result comparable to that of the 30 degree flap deflection. The best results for the vortex plate are seen when the vortex plate

protrudes ahead of the leading edge of the wing. For the vortex plate to be effective, the amount that the plate protrudes from the leading edge of the wing needs to be constant. If the protruded amount is tapered and increasing from the apex, no improvements in the L/D ratio can be ascertained.

### 2.1.2.2 Pneumatic Control

Again, the investigation of control using blowing was two fold. Control investigations started by investigating drag reduction and later applied drag reducing control techniques to stability issues.

The aerodynamic effect associated with blowing a jet spanwise over a wing's upper surface in a direction parallel to the leading edge was investigated by Campbell[34]. For delta wings, arrow wings, and diamond wings with sweep angles of 30 degrees and 45 degrees, spanwise blowing was shown to aid in the formation and control of the leading edge vortices. Campbell demonstrates that blowing rates must increase with spanwise position in order to achieve full vortex lift at a particular spanwise station. The effects of blowing are the generation of larger increases in lift at high angles of attack, improvement of drag polars, and extension of the linear range of pitching moment to higher lift coefficients Lifting efficiency of the spanwise blowing is judged by determining the lift augmentation ratio, $\Delta C_L/C\mu$. This is shown versus angle of attack in degrees in the next figure. As angle of attack increases, the lift effect of the spanwise blowing becomes greater than the effect of the blowing jet thrust acting vertically at about an angle of attack of 15 degrees. The largest augmentation ratio was obtained at the lowest values of blowing rates. As blowing rates increased the lifting efficiency of the jet decreased.

Smaller amounts of blowing increase the jet induced camber effect on the wing, and thus the overall lift at angles of attack above 15 - 16 degree is increased.

Celik, Roberts, and Wood[35] investigate the ability of tangential leading edge blowing to stabilize and control flow asymmetries on a delta wing at high angles of attack. Their experimental effort also investigated the ability to control flow instabilities in the flowfield such as vortex breakdown. For various pitch, roll, and yaw configurations, steady state force, moment, and pressure distribution data was obtained. Pitch configurations included post stall settings. The delta wing model used has a 60 degree leading edge sweep angle. Tangential blowing on the leading edge is implemented by a linearly varying slot which extends from the apex for the entire leading edge. Results obtained indicate that vortical flow can be controlled up to high angles of attack. The roll moment reversed for post-stall angles of attack when compared to the pre-stall measurements. Control reversal due to the reversal of roll moment was diminished by decreasing the effective angle of attack with symmetric blowing. Blowing is found to be effective at different roll and yaw configurations. Asymmetric condition for pre-stall angles of attack can be created by superposing force and moment conditions.

Wong[36] used leading edge tangential blowing with an active control scheme. The blowing scheme used asymmetric blowing from rounded leading edges. By using a symmetric blowing configuration, the wing rock oscillation amplitude was reduced. But, by using the asymmetric configuration and active feedback control, wing rock was damped considerably within one cycle of the limit cycle motion. The success of this technique to modify the wing rock motion is due to the ability of the blowing to control the position of the separation points.

Suarez, et al. [37] conducted experimental free-to-roll tests on a 78 degree swept delta wing. The suppression of wing rock was investigated by using forebody blowing where the forebody is the area on the body preceding the main wing. This study specifically uses the nose area of the model as opposed to the body area ahead of the wing. Several blowing techniques were investigated as a means of suppression. Blowing tangentially aft from side nozzles on the forebody was shown to damp the roll motion at low blowing rates and stop it completely at higher blowing rates. The higher blowing rates created flow asymmetries while eliminating the dynamic hysteresis in the vortices' strength and position. The steady flow asymmetries caused the wing to stop at non-zero roll angles.

The second technique used forward blowing and alternating left - right pulsating blowing This technique was more efficient and could damp the oscillation almost completely at lower blowing coefficients than in the tangential blowing technique. No major vortex asymmetries are induced at lower blowing coefficients.

Greenwell and Wood[38] use tangential leading edge blowing to demonstrate roll moment reversal as reported by Celik, Roberts, and Wood[35]. Similarity of the roll moment reversal to results obtained for high sideslip angles was reported. Blowing on a single leading edge was demonstrated to reduce the effective angle of attack for the blown side while adding an effective sideslip angle. The decrease in effective angle of attack on the blown side yielded increases in the leading edge normal force resulting in a net "blown wing up" rolling moment.

By rounding the leading edges of the wing, blowing air tangent to the surface energized the boundary layer. The jet transfers momentum to the outer flow which delays

the separation of the outer flow itself. By providing control of the separation location, the location and strength of the primary vortex core and its associated feeding sheet can be modified. Also, blowing keeps the vortex system closer to the wing since the effective angle of attack is reduced. The vortex system is able to generate more lift on the blown side of the wing resulting in the blown wing rotating upward.

Bean, Greenwell, and Wood[39] apply tangential leading edge blowing to problems which occur in buffeting of fins or airfoils. Two 60 degree sweep delta wings were used to study buffeting. One wing or fin was rigid and instrumented so that surface pressure data could be obtained. The other wing was flexible to study buffeting response of the wing. The experimentation showed that the buffeting pressure profiles and the response of the delta wing matched each other very closely. Qualitatively, the "effective angle of attack" of the primary vortices was reduced when symmetric leading-edge blowing was used. Symmetric blowing at a constant rate shifted the buffet excitation and response to higher angles of attack. Flow visualization of the flowfield confirmed that the fluid buffeting mechanism was only shifted and not eliminated. With the use of an optimum blowing configuration for each new angle of attack, the response to the buffeting has potential to be completely suppressed.

Crowther and Wood[40] experimentally investigate yaw control through tangential forebody flowing. Force and moment data was measured for angles of attack up to 90° for a number of different slot geometries and locations. It was found that small blowing rates from short slots at the front of the forebody provided larger controlled yawing moments at about $\alpha = 60°$. Using larger slots and larger blowing rates was shown to provide some degree of control up to 90 degrees. Control was demonstrated despite the

loss of coherent vortical flow structures at higher angles of attack. Crowther and Wood identify that yawing moments due to blowing are dependent upon geometry of the body and the slot. Thus for some geometries flowfield coupling between the forebody and wing can lead to unexpected yawing moments and roll moment excursions.

More succinctly, at higher angles of attack, blowing on the left side yields nose-to-left yawing moments and blowing on the right side yields nose-to-right yawing moments. As angle of attack increases throughout the range studied rudder yaw control power decreased while yawing moment available from blowing increases for a given blowing rate.

Discrepancies in the definition of the blowing coefficient showed dependencies of several different parameters. For constant area slots and incompressible flows all definitions are the same, but for different slot areas $C\mu$ describes the trends much more effectively. $C\mu$ is defined as:

$$C\mu = \frac{\rho_{jet} \cdot A_{jet} \cdot (V_{jet})^2}{q \cdot S}$$

Control reversals that occur at low blowing rates are associated with the expected tangential forebody blowing fluid mechanisms reversing. This reversal can be minimized by careful forebody/slot geometry design. Crowther and Wood note that jet mass-flow requirements are within reasonable engine bleed flow levels. Kramer et al.[41] report much the same findings as Crowther and Wood.

Celik, Pedreiro, and Roberts[42] study several forebody blowing schemes to aid in eliminating wing rock. They use tangential forebody blowing to provide lateral control through forebody/wing interactions on a sharp leading edged model. The usefulness of active control through blowing schemes including symmetric, asymmetric, steady, and unsteady blowing was demonstrated. Experimentation showed that the wing rock motion could be suppressed by the steady, symmetric or unsteady, asymmetric tangential forebody blowing. Differences between the symmetric and asymmetric cases were found where asymmetric blowing was found to be very effective.

Ng et al.[43] independently corroborate the findings made by Celik, Pedreiro and Roberts. Tests were conducted on a slender forebody on a 78 degree swept delta wing in a water tunnel. Steady blowing tangential from nozzles at the tip of the forebody was found to be capable of suppressing wing rock. At low blowing rates the motion was attenuated while at high blowing rates the motion was eliminated. Due to the higher blowing rates inducing vortex asymmetries on a time averaged basis, alternating pulsed or unsteady blowing on the left and right sides of the forebody was shown to be effective in suppressing wing rock without creating time-averaged flow asymmetries.

Wong et al.[44] demonstrated experimentally with a free-to-roll wind tunnel model that significant rolling moments could be produced up to an angle of attack of 55 degrees using tangential leading edge blowing. A pair of fast-control servo valves were designed and built to implement an automatic feedback roll control algorithm on a digital controller. Results show that wing rock could be damped at angles of attack up to 55 degrees. By modifying the control algorithm to use asymmetric blowing, wing rock was eliminated in less than one cycle of the limit cycle oscillation. Control reversal between prestall and

poststall angles of attack found previously by other investigators was eliminated using asymmetric blowing with control. Roll command following was shown to be attainable with the use of a feed-forward gain-scheduling control algorithm.

Arena, Nelson, and Schiff[45] investigate problems in directional control of aircraft through pneumatic blowing. An aircraft model with a chined forebody was used to quantify the effectiveness of blowing through a slot in the chine to affect the aircraft's lateral stability. Comparisons to the baseline planform are mode with control deflections of the rudder and with the tail on and off. Results were collected for several blowing coefficient within an angle of attack range from 0° to 75°. Through flow visualization as well as force and moment balance data, results obtained revealed several facts. First, a conventional tail configuration on an aircraft loses it effectiveness at higher angles of attack. In this region, blowing was demonstrated to be an effective alternative since the moment generated by blowing was four times greater at the maximum than the moment of the jet's momentum. Thus, the interaction of the blowing jet with forebody flow is important in generating the large forces and moments on the aircraft. As angle of attack increases, the moments and forces due to blowing increase until the angle of attack forces the blowing fluid mechanism from interaction with the forebody flow of the aircraft. For the planform studied the loss of blowing moment occurred at 60°approximately. The model used was a chined forebody on a 50° swept diamond wing with a single vertical tail. The tail control study revealed that strong interactions exist between the forebody flowfield, the separated wing flow, and the vertical tail. The control authority of the tail is unique for any type of tail configuration. The merit of each tail configuration would have to be investigated before it is implemented in a design. For the specific geometry stated in

certain blowing cases, the lateral controllability was markedly improved. With the conventional rudder along with blowing from the chines, the lateral controllability was almost doubled.

Gittner and Chokani[46] hypothesize that effects of the nozzle exit geometry are important in forebody vortex control when blowing is used. Moksovitz et al. showed the effect of decreasing the vortex asymmetries on the forebody. Therefore, since vortex flow characteristics could be changed by small surface perturbations, nozzle exit geometry may yield additional control of vortical flows. The experimental effort by Gittner and Chokani show that both height and width of the blowing nozzle exit geometry was important. The most effective geometry of these was a low broad nozzle blowing aft along the forebody. Gittner also concluded that the degree of symmetry in the vortical flow before blowing actually moderates the blowing effectiveness.

A survey of past work has shown three methods studied for control of leading edge vortical flows for wing rock. The first method uses a systems approach to quantify the wing rock roll oscillations, identify controllable parameters, and then mathematically arrive at a control algorithm. The most significant result from this type of study revealed that linear feedback of state variables such as roll rate would be sufficient for control of wing rock oscillations. The remaining methods can be categorized as aerodynamic methods where a further understanding of aerodynamics of the flowfield was applied. Within these aerodynamic methods, the two methods of control modify the flowfield through geometric modifications of the planform or through pneumatic methods. Geometric modifications of the planform through the use of vortex flaps, vortex plate, apex flaps, vortex generators, and aerodynamic fences were studied. These methods

prove effective in modifying the location of the separation point of the primary vortices as well as the position and strength of the primary vortices themselves.

Blowing methods implemented tangential leading edge blowing and forebody blowing. Blowing was found to be more successful in controlling leading edge vortex flows when moderate flow rates were used to modify the location of the separation point of the primary vortices and the position and strength of the primary vortices. Higher blowing rates were demonstrated to disturb the flowfield enough to eliminate the effectiveness of the separated flow or in some cases the separated flow itself.

The combination of the three methods show that a control scheme that has the ability to modify the separation point, position, and/or strength of the primary vortices can potentially be effective in controlling leading edge vortical flow found in wing rock oscillations. Control using linear feedback of state variables is sufficient and can be used to determine optimized control algorithms.

CHAPTER 3

METHODOLOGY

## 3.1 Survey of Inviscid, Potential Flow Modeling

A background study of modeling of separated vortical flows is useful in understanding previous successes and limitations of using inviscid, potential flow assumptions. Each type of vortical flow is unique in several aspects; therefore, a discussion of separated vortical modeling only as it relates to sharp leading delta wings will be reviewed. The uniqueness of this flow field is characterized predominantly by the flow separating from the sharp leading edges with the shear layer of the separation coalescing into two primary vortices.

The earliest investigators, such as Legendre[47], Brown and Michael[4], have used potential vortex models to represent steady delta wing flow fields. They found that sharp leading edge delta wings inherently have leading edge separated vortical flow fields. The separation of the flow is caused primarily by viscosity in the boundary layer fixing the separation point at the leading edges. These separated shear layers coalesce into two primary vortices on the suction side of the delta wing. Visser[48] later confirmed through hot wire anemometry that the majority of the vorticity in the flow field is concentrated into the two leading edge vortices. The location of the vorticity on a steady delta wing

34

flow field was determined through calculation of the circulation by performing a line integral around the velocity field data. It was shown that the majority of axial vorticity found in these leading edge vortices is found in the viscous core region of the vortex. The diameter of the core region before vortex burst is on the order of about 5% of the local semi-span. Since the vorticity is concentrated into two regions that are small when compared to the span of the wing, the flow field can be assumed to be inviscid as long as vortex breakdown does not occur. Thus, the two concentrations of vorticity in the primary vortices can be modeled using a potential vortex with a viscous vortex core. Additionally, if the vorticity present at the leading edges is modeled macroscopically, the entire flowfield can be modeled by inviscid fluid mechanics. Consequently, these assumptions are very feasible where vorticity is either neglectible or where it is concentrated. If the vorticity is concentrated and not neglectible then the effects of the vorticity can be modeled macroscopically. For this study, this assumption is good at angles of attack where vortex breakdown is not present on the wing.

In more recent models[49,50,4,5] several additional theories have been used to further simplify the flowfield model. Typically, slender wing theory has been implemented along with a conical flowfield assumption. Slender wing simplifications are implemented by neglecting the gradients of the flowfield in the axial direction when compared to those in the cross flow plane. The slender wing theory is justified since the length of the delta wing is much larger than the thickness.

By using a conical flow assumption, the properties of the flowfield are assumed to be invariant along rays emanating from the apex of the delta wing. The root chord and

local semi span of the wing scale the dimensions of the wing and its aerodynamic characteristics so that the aerodynamic properties are function of y/x and z/x only.

Several conditions must be placed on the use of the conical assumption in a delta wing flowfield. This assumption can be justified experimentally over the forward part of the wing for steady flows. However, as the trailing edge is approached, the conical assumption fails due to trailing edge asymmetries and other effects. Under unsteady conditions, the conical assumption fails for the forward part of the wing because of the unsteady boundary condition. For roll motion the rigid body velocity introduced into the boundary condition is not conical since the rigid body normal velocities vary with the linear distance from the axis of rotation.

The justification for using the conical assumption is provided by Arena[50]. Arena states that due to these reasons discussed above the unsteady flow is not "globally" conical. In experimental efforts by Arena and others, the local flow does not strictly follow conical rays. However, the pressure distributions, vortex positions, and roll moments are qualitatively self-similar. The consequence of only qualitative self similarity is that the flowfield can be solved at any crossflow plane, but the results depend on the chordwise position of that crossflow plane. This dependency is a scale factor. Therefore, the properties have scaled similarity. The scaled factor introduced by the conical assumption will be detailed in the next section.

As can be seen in the following figures, the static position of the vortex cores is three dimensional. As chord station increases, the vortices move to higher and higher positions above the wing. Likewise the vortices move out from the centerline of the wing.
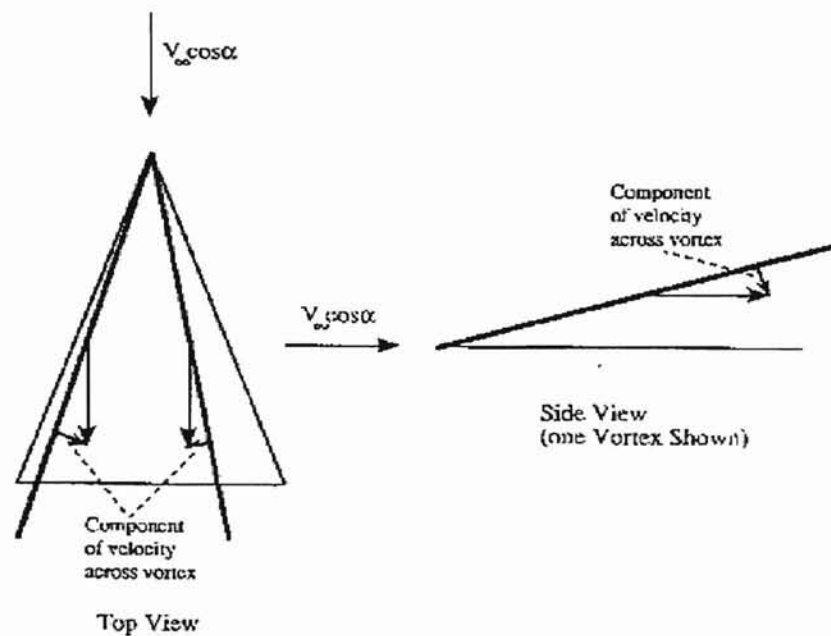
Three Dimensional Trajectories of the Primary Vortices (Arena)

Figure 3.1

The conical assumption is very important because it reduces the solution in three dimensions to a scaled single chord station when coupled to the slender wing assumption. Subsequently, the model is self similar in the axial direction with the similarity being a function of the local chord position and semi-span. After applying the conical assumption, the model is referred to as quasi- three dimensional and not two dimensional because the axial component of velocity is still very much a factor in the model. If the axial component of velocity was not present in the solution, the primary vortex positions would convect normal to the wing surface instead of parallel to the free stream.

The solution of the model thus far would be defined if the mathematical solution were unique. However in addition to the physical problem, the potential of the model thus

far is not unique or more precisely, it is not mathematically single valued. Different investigators have approached this problem from various directions. The major technique is formulated by Brown and Michael[4], and refined by Mangler and Smith[5]. The difference between these techniques is subtle. By observing that a simply connected region would provide a unique solution, a mathematical branch cut emanating from the leading edge and ending at the center of the primary vortex will make the potential of the model single valued. Additionally, a physical mechanism is needed to conduct vorticity from the wing where it is generated to the core of the primary vortices. Brown and Michael model this physical mechanism or "feeding sheet" with a straight branch cut that stretches from the leading edge to the center of the primary vortex on each side. This solves the single valued problem while also providing a model for the physical shear layer coming off the leading edge. A noted liability of using a straight branch cut is that the gradient of the potential is zero across the infinitesimal line that represents the feeding sheet. Since the gradient of potential is zero on either side of the branch cut, the branch cut can sustain no load. This is true of physical shear layers. However, shear layers in this particular situation are physically not straight. They always follow streamlines of the flow. If the mathematical branch cut does not coincide with a shear layer on a streamline, then additional error is introduced into the model. Mangler and Smith recognized this liability and use the same technique except that their feeding sheet is curved and follows the stagnation streamline from the leading edge to the center of the primary vortex. This second technique is more accurate in that a force cannot exist across a shear layer or a streamline. Using Brown and Michael's linear model, a force would exist on the branch cut.
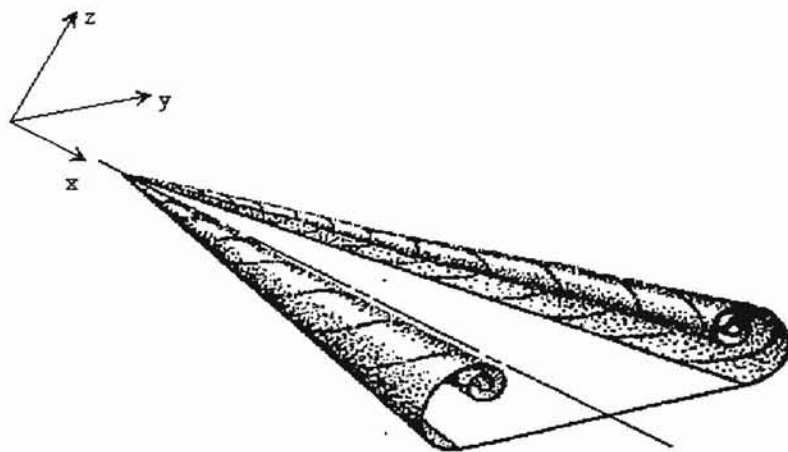
a) actual flowfield
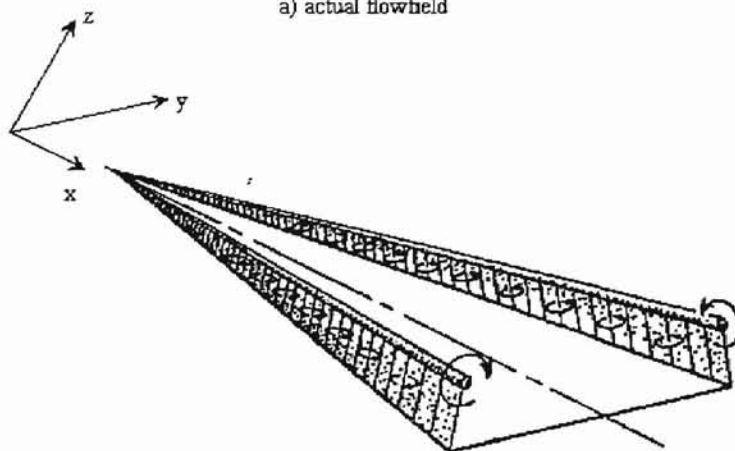


b) approximated flowfield

Assumed and Approximated Flowfield Sketches
(Brown and Michael 1955)

Figure 3.2

The model presented here uses the linear branch cut for simplicity in its implementation since the curved branch cut added additional complexity to the model and yielded little in terms of accuracy. When using a branch cut that does not follow a streamline, the position of the feeding sheet must be found by iterating the flowfield solution until no force exists across each feeding sheet. From the crossflow plane determined by the using the conical assumption, no forces can exist on the primary vortices either. In this effort, the model enforces the no force condition on the branch cut and the primary vortices together for each side. With the specification of the no force conditions, the steady state model of a separated vortical flowfield is complete, and the solution will be mathematically unique. The model showing the linear branch cuts along with the force balance can be seen in Figure 3.3.
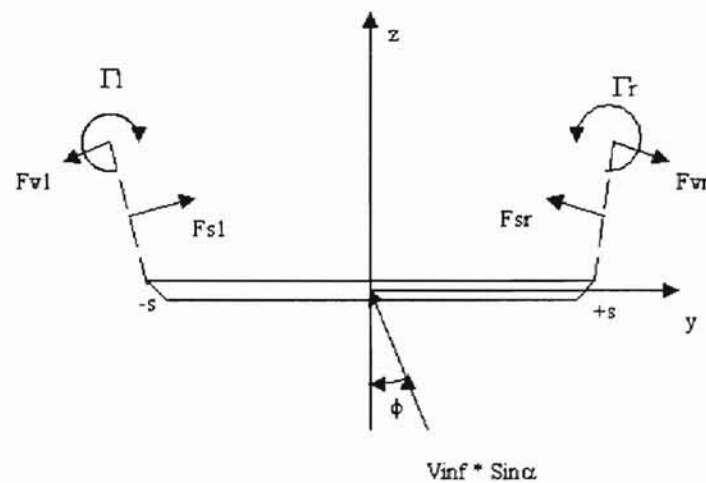
Delta Wing Crossflow Plane with Branch Cut

Figure 3.3

Arena and Nelson[50] extended the use of the potential model with linear feeding sheets by applying it to the unsteady flowfield. Solving a dynamically changing flowfield is more complicated than solving a steady state flowfield at discrete time intervals. Much of the extension of the potential model to the unsteady flowfield case is not intuitive. For example, the potential of the flowfield at each point is not constant as it is in the steady case. The potential of the flowfield varies with time at each location. Despite additional complications, Arena and Nelson have shown that the essential characteristics of the unsteady delta wing still can be captured by modeling only the primary flow characteristics, namely the primary vortices. The model developed by Arena and Nelson used a conformal mapping technique to solve the flowfield. The conformal mapping can provide an exact solution for a given model; however, the thickness of the wing was not included due to the complexity of transforming the "thick" model into the complex plane.

The solution to the present model will be obtained by using a panel technique where the body geometry represented by a distribution of constant strength sources and vortices. The source strengths for each panel will vary while the vortex strengths will be constant and equal for all panels. This solution method will allow the delta wing to have an arbitrary thickness distribution allowing investigation of variations in planform geometries.

## 3.2 Solution of Mathematical Model

The mathematical representation and solution of the unsteady delta wing model is detailed in the following three categories:

1. Definition of Governing Equations

2. Governing Equations Solution Method

3. Extension of Model to Unsteady Motion

### 3.2.1 Definition of Governing Equations

The model is mathematically defined by stating conservation of mass along with simplifications such as incompressibility, irrotationality, and wing slenderness as it applies to the delta wing flowfield.

### 3.2.1.1 Unsteady Conservation of Mass

The major assumptions of the model are that the flowfield is incompressible, inviscid, and unsteady. The continuity equation reduces to yield the governing equation as follows. The continuity equation is

$$\nabla \cdot \vec{q} = 0 \qquad \text{where} \quad \vec{q} = \langle u, v, w \rangle \qquad (\text{Eq. 1})$$

Since the flowfield is irrotational,

$$\nabla \times \vec{q} = 0$$

A potential function can be defined such that

$$u = \frac{\partial \Phi}{\partial x} \quad \text{and} \quad v = \frac{\partial \Phi}{\partial y} \quad \text{and} \quad w = \frac{\partial \Phi}{\partial z}$$

Substituting the potential function definition for the velocity components into equation 1,

$$\frac{\partial^2 \Phi}{\partial x^2} + \frac{\partial^2 \Phi}{\partial y^2} + \frac{\partial^2 \Phi}{\partial z^2} = 0$$

The governing equation of the flowfield is then

$$\nabla^2 \Phi = 0 \qquad\qquad (\text{Eq. 2})$$

### 3.2.1.2 Slender Wing Assumption

The next assumption made in developing the model is that the wing is a slender wing. The slender wing assumption states that gradients with respect to the x direction are negligible compare to the y and z directions in the crossflow plane. In other words, the crossflow plane is dominant.

$$\frac{\partial}{\partial x} << \frac{\partial}{\partial y}, \frac{\partial}{\partial z}$$

### 3.2.1.3 Conical Assumption

A dominant crossflow coupled with a conical flowfield assumption allows the crossflow planes of the delta wing to have self-similarity. With these two assumptions, the governing equation reduces to two dimensions in the crossflow plane. Note however that the solution is still quasi-three dimensions since the axial component of velocity is still present.

$$\nabla^2 \Phi \approx \frac{\partial^2 \Phi}{\partial y^2} + \frac{\partial^2 \Phi}{\partial z^2} = 0 \qquad\qquad (\text{Eq. 3})$$

In Figure 3.1, the geometry of the wing is defined as having a local semi-span, s, and a sweep angle, $\Lambda$. Furthmore, $\varepsilon = 90° - \Lambda$. For conical variables anywhere on the wing, the chord position is scaled by the local semi-span.

$$x^* = \frac{x}{s} = \tan \varepsilon$$

The crossflow dimensions are nondimensionalized by applying the conical assumption.

$$y^* = y/s \quad \text{and} \quad z^* = z/s$$

### 3.2.1.4 Boundary Conditions

To obtain the solution to the 2D Laplace's equation for flow on a body, boundary conditions must be stipulated on the boundary itself and in the far field at infinity. The boundary condition on the boundary is such that the flow must be tangent to the surface of the body. The far field boundary condition states that the perturbation velocity in the flow field must be zero at infinity. Stated another way, the total potential of the flowfield at infinity must be equal to the potential of the freestream itself.

On the surface of the body,

$$\nabla \Phi \cdot \bar{n} = V_n$$

where $n$ is a unit vector normal to the surface of the body and $V_n$ si the normal velocity of the rigid body on the surface of the wing. For steady conditions, $V_n = 0$.

In the far field at infinity,

$$\nabla\Phi = \vec{q}_\infty \sin\alpha$$
$$r\to\infty$$

### 3.2.2 Flowfield Solution

The solution of the conical, slender wing Laplace's equation is obtained by superposing potential singularity solutions in the crossflow plane along with laws governing vorticity generation and shedding.

### 3.2.2.1 Singularity Solution Superposition

The singularity solutions are distributed along the surface of the wing itself by discretizing the wing geometry into a number of linear panels that approximate the actual shape. The wing is discretized using cosine spacing to yield better resolution of the flowfield on the geometry at the leading edges. Cosine spacing allocates the panel end points according to a constant angle of $\Delta\beta = 2\pi/m$ where m is the number of panels. The independent coordinate of the end points is described by

$$x = \frac{c}{2}(1 - \cos\beta)$$

while the dependent coordinate is determined by the desired geometry. By distributing a singularity solution on each panel, the flowfield about any arbitrary shape can be found.

Each panel also has a collocation point defined at its center. The collocation point is the geometric location where the boundary conditions are enforced. For this study, the flow tangency boundary condition for each panel will be satisfied at the collocation point of each panel by requiring the sum of the velocities generated by all of the singularity

solutions to be equal to the normal velocity of the wing. The boundary condition at infinity states that the perturbation velocities induced by the wing must be zero. This boundary condition will be satisfied by choosing singularity solutions that automatically satisfy the far-field boundary condition.

This method is known as a panel method. In contrast to the conformal mapping technique, the panel method technique allows a solution to be obtained that can account for thickness of the geometry. However, the panel method is an inexact solution to an inexact model whereas conformal mapping is an exact solution to an inexact model. Therefore, for a thick wing, a trade-off exists between complexity of the transform in complex variables and the errors introduced by using a panel method.

A number of combinations of singularity solutions work in this application. So, the choice of the actual singularity solutions to be used is somewhat arbitrary. For this model, constant strength source and vortex distributed singularity solutions are used on the boundary to approximate the geometry of the delta wing in the freestream flow. The equation for the velocity at a point due to a constant strength distributed source is shown below along with the velocity due to a constant strength distributed vortex. The derivation of these equations can be found in Katz and Plotkin[51].

After applying the conical assumption, the velocity due to a constant strength distributed source in local panel coordinates is given by the following equations:

$$u_p^* = \frac{\sigma^*}{4\pi}\ln\left[\frac{\left(y^* - y_1^*\right)^2 + z^{*2}}{\left(y^* - y_2^*\right)^2 + z^{*2}}\right]$$

$$w_p^* = \frac{\sigma^*}{2\pi}\ln\left[\tan^{-1}(\frac{z^*}{y^* - y_2^*}) - \tan^{-1}(\frac{z^*}{y^* - y_1^*})\right]$$

where

$$y^* = \frac{y}{s}$$

$$z^* = \frac{z}{s}$$

$$\gamma^* = \frac{\gamma}{V_\infty \sin\alpha}$$

$$\sigma^* = \frac{\sigma}{V_\infty \sin\alpha}$$

$$\Gamma^* = \frac{\Gamma}{V_\infty \sin\alpha}$$

The velocity due to constant strength distributed vortex in local panel coordinates is:

$$u_p^* = \frac{\gamma^*}{2\pi}\left[\tan^{-1}\left(\frac{z^* - z_2^*}{y^* - y_2^*}\right) - \tan^{-1}\left(\frac{z^* - z_1^*}{y^* - y_1^*}\right)\right]$$

$$w_p^* = \frac{\gamma^*}{4\pi}\left[\ln\frac{(y^* - y_2^*)^2 + (z^* - z_2^*)^2}{(y^* - y_1^*)^2 + (z - z_1^*)^2}\right]$$

where (y,z) are the coordinates of the collocation points, $(y_1, z_1)$ are the coordinates of the counter-clockwise most end, and $(y_2, z_2)$ are the coordinates of the clockwise most end.

The velocities due to the free vortices used to model the primary vortices are

$$u_v^* = \frac{\Gamma^*}{2\pi} \cdot \frac{(z^* - z_0^*)}{(z^* - z_0^*)^2 + (y^* - y_0^*)^2}$$

$$w_v^* = \frac{-\Gamma^*}{2\pi} \cdot \frac{(y^* - y_0^*)}{(z^* - z_0^*)^2 + (y^* - y_0^*)^2}$$

The center of the potential vortex origin is located at point $(y_0, z_0)$ while the point of interest is located at the point $(y, z)$.

The arbitrarily chosen singularities of a distributed constant source and a distributed potential vortex are solutions of Laplace's governing equation individually. Using superposition, a linear combination of both of the individual solutions can be found such that a particular set of boundary conditions is satisfied. Since these singularity solutions also automatically satisfy the far field boundary condition, the remaining conditions to be satisfied are the boundary condition of flow tangency on the wing along with specification of circulation in the flowfield. The boundary condition on the surface of the wing is enforced at the collocation point of each panel.

The solution scheme depends upon whether the equations governing the circulation in the flowfield are linear or non-linear. The equations specifying the flow tangency on the panels are linear. As a result, all of the flow tangency equations along with the linearized circulation equations can potentially be placed in a matrix form and

solved by LU decomposition, a method of inverting ill conditioned matrices. The solution of the linear equations is iterated until the non-linear governing equations are satisfied.

### 3.2.2.2  Flow Tangency and Influence Coefficients

The tangential flow equations are used to develop an influence coefficient matrix to numerically solve flow tangency on the surface of the delta wing. The influence coefficient matrix is a matrix containing the linear governing equations that either fully or partially define the solution depending on whether nonlinear governing equations are used. If non-linear equations define the system, the solution is only partially defined by using the influence coefficient matrix. To complete the solution, the linear set of equation must be iterated until the non-linear governing equations are satisfied. This basic scheme can be used for steady and unsteady solutions. The influence coefficient matrix is the set of equations that state that the velocity due to the sum of the singularity distributions on all of the panels vectorially dotted with the normal panel vector must equal zero. In mathematical notation, the boundary condition is satisfied at n points and is written as

$$\sum_{j=1}^{n} \vec{q}_{ij} \cdot \vec{n}_i = 0 \qquad \text{i = integers from 1 to n}$$

also

$$\vec{q}_{ij} \cdot n_i = a_{ij} \cdot \gamma_j + b_{ij} \cdot \sigma_j$$

where $q_{ij}$ is the velocity vector induced by singularity distribution j on panel i. The influence coefficients $a_{ij}$ and $b_{ij}$ are the normal velocities induced on panel i by a vortex and source distribution each of unity strength at panel j. The influence coefficients are dependent entirely upon geometry of the wing. By calculating an influence coefficient matrix using unity strengths, the unique solution of $\gamma$ and $\sigma$ can be determined such that

the zero normal flow boundary condition is satisfied at all the collocation points. However, this linear solution will not be unique if only the boundary condition influence coefficients are specified.

To ensure that a unique linear solution exists, additional physical parameters must be written that specifiy the circulation. The Kelvin condition ensures that the vorticity generated on the wing is shed into the wake. Additionally, a Kutta condition for each separation point must be included in the solution. For an inviscid model, a Kutta condition enforces the global characteristics of separation.

### 3.2.2.3 Kutta Condition

By observation of the flowfield, it is assumed that the only effect of viscosity in the problem is to fix the separation points at the leading edges. Each Kutta condition models the effect of viscosity and forces a stagnation point to be located at the sharp point of each leading edge. A Kutta condition can either by unsteady or steady. However, an unsteady Kutta condition is nonlinear making its inclusion in the influence coefficient matrix impossible if not linearized. In this effort, a steady Kutta condition is used because the reduced frequencies characteristic in delta wing motions are low. The use of the steady Kutta condition has been demonstrated previously by Katz and Plotkin[57]. By the Kutta condition being steady, the solution scheme is simplified because the steady equation is linear whereas the unsteady Kutta condition is nonlinear. The linearity of the Kutta conditions allow them to be included in the matrix solution along with the equations stating flow tangency. The difficulty in using an unsteady Kutta condition can be seen.

The circulation or vorticity is determined by a unique solution of the linear equations. If this set of equations is not unique, then how can the proper circulation be found?

The stagnation point on each leading edge is modelled mathematically by observing that the vorticity at the leading edge must be zero. A corollary is the flow at the leading edge must be irrotational; therefore, the tangential velocities on either side of the leading edge must be equal. A second corollary states that the pressure must be equal on either side of the separating shear in order for it to not sustain a load. Again the tangential velocities must be equal for the pressures to be equal. The Kutta equations are as follows:

$$u_{P_1} = u_{P_n}$$

$$u_{P_{n/2}} = u_{P_{(n/2+1)}}$$

Note that these velocities are local panel velocities. They must contain velocities due to all components on the model, n source panels, n vortex panels of constant strength, 2 potential vortices, and the free stream.

### 3.2.2.4 Kelvin Condition

The final equation that is included in the linear portion of the solution is the Kelvin condition. The Kelvin condition ensures that the vorticity generated on the wing is shed into the wake at each time step. The difficulty that arises with the Kutta condition is not present since the Kelvin condition is linear for both the steady and unsteady cases. The condition is represented by

$$\sum_{i=1}^{n} \gamma_i \cdot dl_i = \Gamma_l + \Gamma_r$$

The solution to the linear portion of the model is formulated in the following manner. Flow tangency equations are placed in the first m rows of the matrix. One equation is written for each panel's collocation point. The coefficients $a_{11}$ through $a_{n,m+3}$ are influence coefficients which when multiplied by the corresponding source or vortex strength reflect the velocity due to $n^{th}$ source or vortex strength on the $m^{th}$ collocation point. A linearized form of the kutta condition for the left and right leading edges to ensure no shear force at the separation point. The Kelvin condition completely determines the linear solution by specifying that the generated circulation is shed into the wake. The right hand side (RHS) of the solution for the first n rows is simply the unsteady boundary condition enforced at the collocation point. For the unsteady condition, the normal velocity at each of the collocation points is specified to prevent flow through the corresponding panel. The right hand side for the kutta conditions is remainder of the terms from the linearized equation, namely the free stream velocities. The right hand side for the Kelvin condition is simply zero.

$$\begin{bmatrix} a_{11} & \cdots & a_{1n} & \cdots & a_{1,n+3} \\ & \ddots & & & \\ & & \ddots & \vdots & \vdots \\ & & & \ddots & \\ a_{n1} & \cdots & a_{nn} & \cdots & a_{n,n+3} \\ \hline \multicolumn{5}{c}{Right.Kutta.Condition} \\ \multicolumn{5}{c}{Left.Kutta.Condition} \\ \multicolumn{5}{c}{Kelvin.Condition} \end{bmatrix} \times \begin{bmatrix} \sigma_1 \\ \vdots \\ \vdots \\ \vdots \\ \sigma_n \\ \gamma \\ \Gamma_r \\ \Gamma_l \end{bmatrix} = \begin{bmatrix} RHS_1 \\ \\ \vdots \\ \\ \\ \vdots \\ \\ RHS_{n+3} \end{bmatrix}$$

## 3.2.2.5 Zero Force

An actual delta wing has a flow field such that a shear layer emanates from the leading edge and follows a streamline. The shear layer must follow a streamline in the flow since a shear layer cannot sustain a force. The shear layer separating from the leading edge rolls up to form the primary vortices. For simplicity, the feeding sheet or shear layer that lies between the leading edge and the free vortex is approximated as linear. A depiction of this can be seen in Figure 3.4.
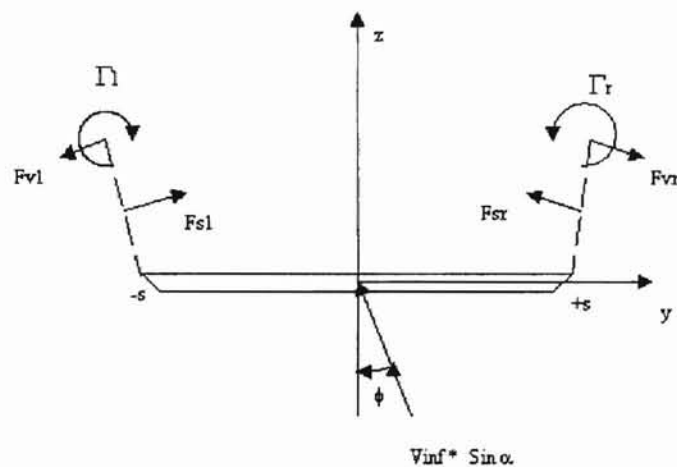
Figure 3.4 Crossflow plane with branch cut forces

This model by itself violates the zero force condition as discussed previously, but when coupled with the free vortex, the zero force condition can be enforced for both the feeding

sheet and the free vortex. A mathematical branch cut joins each leading edge of the wing with the primary free vortex on the same side to make the solution of the flowfield potential single valued. Zero force is obtained by summing the forces acting on each branch cut as follows.

$$\vec{F}_{vl} + \vec{F}_{sl} = 0$$

$$\vec{F}_{vr} + \vec{F}_{sr} = 0$$

The forces which act at the center of the primary vortices are the forces due to the relative velocity across the vortex line. The force is given by

$$\vec{F}_v = \left(\rho \vec{V}_{rel}\right) \times \left(\vec{\Gamma}_v\right)$$

$$\vec{\Gamma}_v = \Gamma \vec{i}$$

and $U_{rel}$ is the relative velocity across the vortex tube. Since the cross product of the direction denoted by $\vec{i}$ is zero when crossed with itself, only the crossflow components of velocity are important. The components that are perpendicular can be seen in Figure . These components are perpendicular due to the conical assumption. The component in the z direction is given by

$$V_z = V_\infty \cos\alpha \tan\theta_z = V_\infty \cos\alpha\left(\frac{z}{x}\right)$$

Likewise the component in the y direction is given by

$$V_y = V_\infty \cos\alpha \tan\theta_y = V_\infty \cos\alpha\left(\frac{y}{x}\right)$$

Transforming to conical variables yields,

$$V_z = V_{\infty}z^* \cos\alpha \tan\varepsilon$$

$$V_y = V_{\infty}y^* \cos\alpha \tan\varepsilon$$

$$V_x \approx V_{\infty}$$

Extending these equations to the unsteady case, the vortex itself is free to move; therefore, the vortex motion must be subtracted to get relative velocity.

$$V_z = V_{\infty}z^* \cos\alpha \tan\varepsilon - \frac{(z_v^* - z_0^*)}{\Delta t}$$

$$V_y = V_{\infty}y^* \cos\alpha \tan\varepsilon - \frac{(y_v^* - y_0^*)}{\Delta t}$$

where $(y_0, z_0)$ identifies the leading edge of the wing on the same side as the vortex.

Therefore,
$$\hat{V}_{rel} = V_x\bar{i} + V_y\bar{j} + V_z\bar{k}$$

and

$$\bar{F}_v = \rho\Gamma_v\left[ V_{\infty}\cos\alpha \tan\varepsilon(y^*\bar{k} + z^*\bar{j}) - \frac{(y_v^* - y_0^*)}{\Delta t}\bar{k} - \frac{(z_v^* - z_0^*)}{\Delta t}\bar{j} \right]$$

The remaining force is the unsteady force due to the discontinuity of potential across the feeding sheet. This is computed by integrating the pressure differential across the feeding sheet.

$$\bar{F}_s = \left[ \int_{z0}^{zv}\Delta C_P \frac{1}{2}\rho V_{\infty}^2 dz \right]\bar{j} + \left[ \int_{y0}^{yv}\Delta C_P \frac{1}{2}\rho V_{\infty}^2 dy \right]\bar{k}$$

The unsteady change in pressure is

$$\Delta C_p = \frac{p_{above} - p_{below}}{\frac{1}{2}\rho V_{\infty}^2} = -\frac{(\Delta\Phi_s)_x}{\frac{1}{2}V_{\infty}^2}V_{\infty}\cos\alpha - \frac{(\Delta\Phi_s)_t}{\frac{1}{2}V_{\infty}^2}$$

Substituting the change in the coefficient of pressure into the equation above yields,

$$\bar{F}_s = \left[\int_{z0}^{zv}\left(-(\Delta\Phi_s)_x V_\infty \cos\alpha - (\Delta\Phi_s)_t\right)\rho dz\right]\bar{j} + \left[\int_{y0}^{yv}-(\Delta\Phi_s)_x V_\infty \cos\alpha - (\Delta\Phi_s)_t \rho dy\right]\bar{k}$$

or

$$\bar{F}_s = \left[\int_{z0}^{zv}\left(-\frac{\partial\Gamma_v}{\partial x} V_\infty \cos\alpha - \frac{\partial\Gamma_v}{\partial t}\right)\rho dz\right]\bar{j} + \left[\int_{y0}^{yv}\left(-\frac{\partial\Gamma_v}{\partial x} V_\infty \cos\alpha - \frac{\partial\Gamma_v}{\partial t}\right)\rho dy\right]\bar{k}$$

$$\bar{F}_s = \rho\left[\left(-\frac{\partial\Gamma_v}{\partial x} V_\infty \cos\alpha - \frac{\partial\Gamma_v}{\partial t}\right)(z_v^* - z_0^*)\bar{j} + \left(-\frac{\partial\Gamma_v}{\partial x} V_\infty \cos\alpha - \frac{\partial\Gamma_v}{\partial t}\right)(y_v^* - y_0^*)\bar{k}\right]$$

Equating the feeding sheet force to the force on the vortex yields <u>two orthogonal equations for each side.</u>

In the y* direction,

$$\left(-\frac{\partial\Gamma_v}{\partial x} V_\infty \cos\alpha - \frac{\partial\Gamma_v}{\partial t}\right)(z_v^* - z_0^*) + \Gamma_v\left[V_\infty z^* \cos\alpha \tan\varepsilon - \frac{(z_v^* - z_0^*)}{\Delta t}\right] = 0$$

In the z* direction,

$$\left(-\frac{\partial\Gamma_v}{\partial x} V_\infty \cos\alpha - \frac{\partial\Gamma_v}{\partial t}\right)(y_v^* - y_0^*) + \Gamma_v\left[V_\infty y^* \cos\alpha \tan\varepsilon - \frac{(y_v^* - y_0^*)}{\Delta t}\right] = 0$$

3.2.2.6 Steady Convergence

Since the zero force condition is nonlinear, the condition is satisfied outside of the linear solution. The linear solution is iterated until the zero force condition on both pairs of feeding sheets with the potential vortex is satisfied. Zero force is satisfied by

computing the velocity at the old vortex position. This velocity is multiplied by the time step to move the vortex to its new position. Iteration occurs until both vortices have converged on the actual position. The convergence criteria is computed by calculating the norm of the differences between the old and new positions.

$$norm = \sqrt{(vp_{old}(left) - vp_{new}(left))^2 + (vp_{old}(right) - vp_{new}(right))^2}$$

A total of m+5 equations and m+5 unknowns completely specify the problem where m is the total number of panels used. The equations are as follows: n equations stating zero normal flow, left Kutta condition, right Kutta condition, Kelvin condition, zero force specification on the left feeding sheet and vortex, and zero force specification on the right feeding sheet and vortex. With the problem being completely specified, the system of equations is solved by using the nonlinear equations as a convergence criteria for an iterative solution. Within each iteration, the linear equations are solved by LU decomposition. This static solution is iterated to converge upon the correct primary vortex positions. The no-force condition is applied after each solution within the iteration step to predict the new refined position of the vortices.

### 3.2.3 Extension of Model to Unsteady Motion

Extension of the model to include unsteady motion requires changes to the boundary conditions as well as the zero force condition and pressure calculations.

3.2.3.1 Rigid Body Equation in Roll

Once the static solution to the wing rock problem has been found, the unsteady-dynamic coupled solution can be started. From the flow solution for the delta wing, the initial roll moment is calculated for the wing. From rigid body dynamics, a roll velocity can be calculated by assuming a value of inertia for the wing in roll. The dynamic equation is as follows

$$L_{aero} = I_x \ddot{\phi}$$

The new roll angle is calculated by using a forward difference technique such that

$$\phi_{new} = \phi_{old} + \frac{L_{aero}}{I_x}(\Delta t)^2 \qquad (\text{Eq. 5})$$

3.2.3.2 Unsteady Boundary Conditions

It is important to note again that the boundary conditions are different for the dynamic solution. The no-flow boundary condition used on the wing now has another velocity to be taken into account. The resultant velocity normal to each panel still must be zero, but the resultant velocity includes a term for the velocity of the body. The new boundary condition is then stated as follows:

$$\nabla \Phi = \vec{q}_{body} \cdot \vec{n}$$

where $q_{body}$ is the velocity of the wing itself. In the static case, $q_{body}$ is zero; therefore, the dynamic boundary condition reduces to the static boundary condition.

### 3.2.3.3 Unsteady Zero Force

A similar solution technique to that used to find the static flowfield is then used to find the proper vortex positions. The difference between the two techniques is that the position of the vortices is found by using a forward difference in time technique instead of an iteration scheme as in the first technique.

At each time step of the dynamic solution, a new roll moment must be calculated. The roll moment is a function of the surface pressures, but the surface pressures are not calculated using the static form of Bernoulli's equation. The dynamic pressure differs from the static pressure because the potential of the model is not constant through time. The potential, $\Phi$, changes with time by an amount $d\Phi/dt$. The equation for unsteady pressure is as follows:

$$\Delta C_p = \frac{P_\infty - p}{\frac{1}{2}\rho V_\infty^2} = -\frac{1}{V_\infty^2}\nabla^2\Phi - \frac{2}{V_\infty^2}\frac{\partial \Phi}{\partial t}$$

### 3.2.4 Unsteady Vortex Flow Control

A simple wing rock suppression technique has also been designed into the model. The bevels on the delta wing have been implemented so that they can be rotated about their lower corners. This allows the use of the leading edges to simulate vortex flaps. The vortex flaps modify the characteristics of the separation and therefore the primary vortex position and strength. Furthermore, the position and strength of the vortices are crucial to

specifying the roll moment. Once the roll moment is affected in some way, any arbitrary control algorithm can then be investigated to control the dynamic motion of the wing.
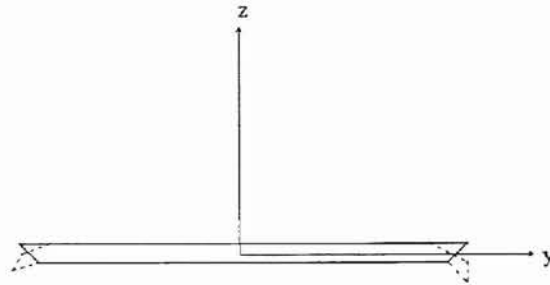
Figure 3.1 Delta Wing Cross Sectional Geometry with Vortex Flaps.

# CHAPTER 4

## RESULTS

Once the model of the wing rock phenomenon was developed, the model was validated statically and dynamically against efforts by Arena[49] and others. Separated vortex control methods were implemented only after the model predicted the limit cycle oscillation qualitatively. These methods demonstrate the flexibility of this type of model to evaluate proposed control methods.

### 4.1 Static Model Validation

For a delta wing at an angle of attack of 30 degrees and a sweep angle of 80 degrees, static tests were run to validate the model with experimental data obtained by Arena[1]. The delta wing had a thickness to span ratio of 4.25%. All of the primary flowfield characteristics have been qualitatively captured for conditions where vortex breakdown is not present near the wing.

Previous delta wing studies have shown static roll moments to be a function of roll angle. A comparison of the inviscid delta wing model to experimental data can be made by studying three fundamental variables that combine to result in a static roll moment for the wing. These three variables are the lateral and normal positions of the primary vortices and primary vortex strengths. In the comparison of lateral position versus roll angle shown in Figure 4.1, the prediction of the upper vortex is closer to experimental
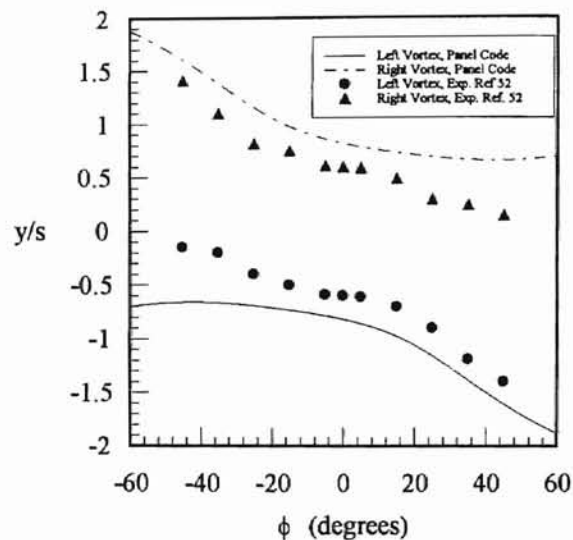
Figure 4.1  Static Lateral Primary Vortex
Variation

value than the lower vortex where the upper vortex is the right vortex when the wing is at

a negative roll angle.

The normal position of the primary vortices is shown in Figure 4.2.  The figure

shows qualitative agreement with experimental values; however,  with the entire vorticity

assumed to be located at the center of vorticity, the computational values are shifted by a

bias of about 12% of the semi-span.  For static cases, the vortex corresponding to the

wing which is down moves closer to the wing.  The variation of strength is shown in

Figure 4.3. These variations in the lateral and normal position and the strength of the

vortices combine to cause a variation in roll moment with roll angle.  No data could be

found to compare against; however, the combination of these factors can be seen in

Figure 4.4.  The sectional roll moment has been computed by integrating the effects of the

primary vortices on the wing.  The effects are dependent upon the position and strength of

the primary vortices.  The panel model captured the experimental sectional roll moment
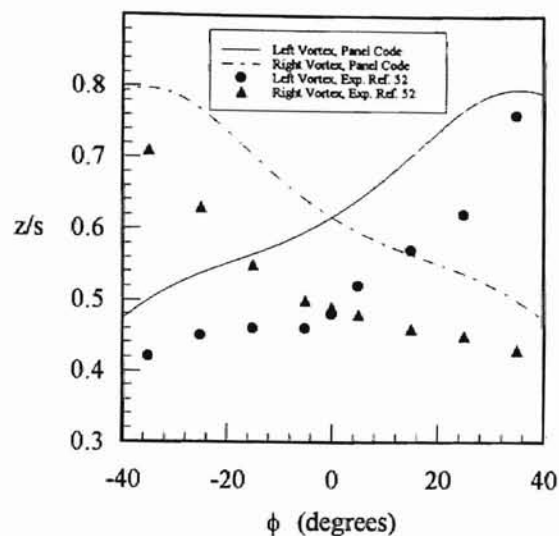
Figure 4.2 Static Normal Vortex Position
Variation

well within the range of roll angles, $-25° < \phi < 25°$. Beyond roll angles of $-25°$ or $25°$ the

model over predicts the experimental data because of the limiting assumptions used in

developing the model.

The assumption that has the greatest effect is the inviscid flowfield assumption. By

adopting the inviscid assumption, the inertia forces are assumed only to be much greater

than the viscous forces. In other words, the Reynolds number is assumed to be high. As

the Reynolds number increases, the flow field transitions from laminar to turbulent. The

comparison to Arena's data shows the sensitivity of delta wing flows to Reynolds number.

Arena's data was obtained at a Reynolds number of 400,000. Previously, Hummel's[52]

flow regime at a Reynolds number of 900,000 was determined to be laminar. Thus, the

experimental flow is laminar for this case. The result is that the flow does not have the

energy needed to traverse the adverse pressure gradient on the top surface of the wing.

Secondary separation forms beneath the primary vortex on each side increasing the
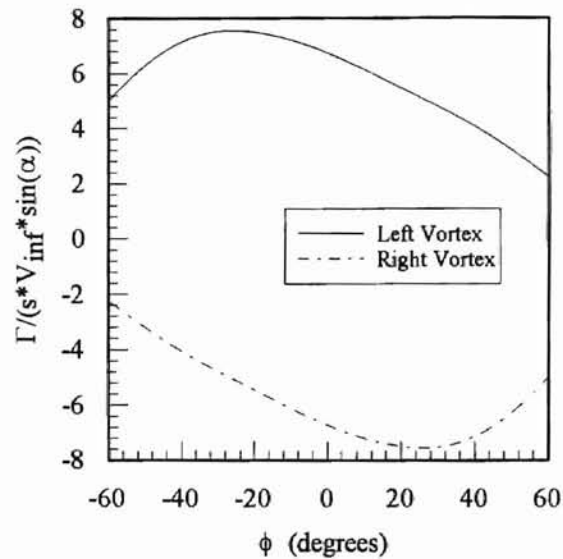
Figure 4.3 Static Primary Variation of Vortex
Strength

surface pressure on the top of the wing. If the boundary layer was turbulent, the adverse

pressure gradient could be overcome keeping the pressure lower on the top surface of the

wing. So, the over prediction is due to the increased region of secondary separation since

the surface boundary layer is laminar. The model prediction would be closer to the case

where the boundary layer is turbulent. This is shown by the computational coefficient of

pressure distribution for a typical delta wing for roll angles of zero and fifteen degrees in

Figure 4.5. The computational pressure distribution agrees quantitatively with the

experimental data for the phi = 0.0 case. The experimental data was taken at an chord

station of $x/c_r = 0.3$. Notice the high suction peaks due to the primary vortices on the top

surface of the wing. The higher suction peaks of the computational data are diminished in

the experimental data. The discrepancy can be attributed to the formation of secondary

vortices in the laminar experimental flow regime. As roll angle increases, the suction peak

on the side of the wing that is rotating downward has a higher coefficient of pressure due
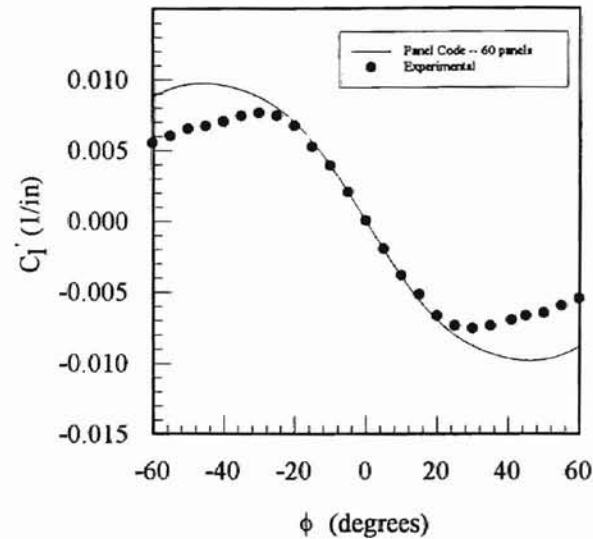
Figure 4.4  Static Sectional Roll Coefficient Variation

to the change in position and strength of the vortex.  The suction peak on the opposite side actually decreases denoting the corresponding vortex has moved further from the surface of the wing as was shown in Figure 4.3.

The agreement of the various parameters fundamental to static delta wing flow fields with experimental data demonstrated the feasibility of the model to capture the static characteristics of the fundamental parameters.  By combining these fundamental parameters of position and strength of the primary vortices to form a static sectional roll moment, the capability of the model is further corroborated by the agreement with experimental static sectional roll moment in Figure 4.4.
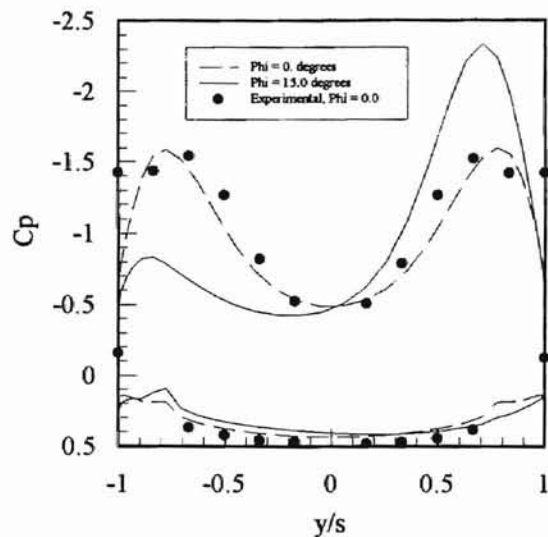
Figure 4.5  Conical Pressure Distribution

## 4.2  Dynamic Model Validation

Once the model was validated statically, the model was expanded to explore and validate the dynamic characteristics.  To ensure valid initial conditions, a steady state solution was first found for a specific angle of attack and roll angle.  Just as in the steady case,  the primary vortex position was iterated upon until no force existed on the linear vortex sheets.  When the correct static position was found, the wing was released in the lateral mode to roll independently.  The initial angular rate of motion at release was zero. The other five degrees of freedom are fixed for any given case.  The unsteady solution of roll angle and vortex position and strength were calculated by integrating the unsteady pressure over the wing and then marching the solution to the next solution in time by a factor of $\Delta t$, typically on the order of 0.05 seconds.

It is important to note that vortex breakdown on the wing is not necessary for the wing rock limit cycle oscillation to occur. Arena and Nelson[1,2,9] have shown that at higher angles of attack where breakdown is present, additional damping is generated due to the time lag in breakdown position. Currently, the model does not account for vortex breakdown. Consequently, the dynamic model cannot accurately predict wing rock amplitudes when any amount of vortex breakdown is occurring on the wing itself. This limits the model to angles of attack less than 36 degrees for an 80° swept delta wing.

Upon release from a perturbed condition, the model demonstrated wing rock lateral oscillations. The steady state amplitude of the wing rock oscillation is compared to the experimental wing rock in Figure 4.6. When the computational envelope is compared to experimental studies by Arena and Nelson[50], Nguyen, Yip, and Chambers[53], and Levin and Katz[54] the onset of the wing rock oscillations have decreased by an angle of attack of
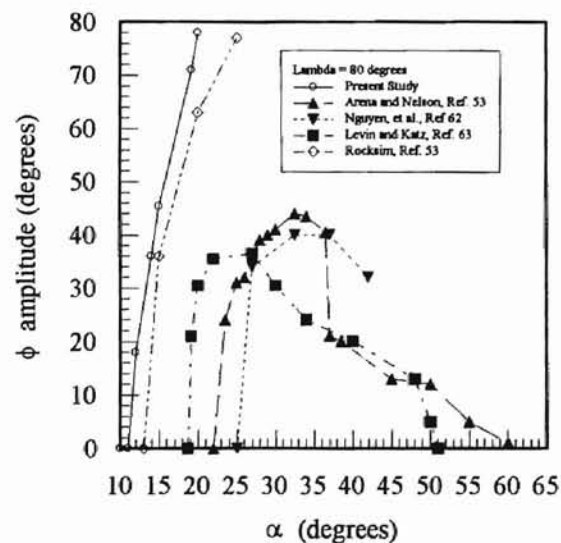


Figure 4.6 Wing Rock Amplitude Envelope

10 degrees. Onset is described as the lowest angle of attack for which steady state limit cycle oscillations occur. This bias in the onset may be due to the assumption that the primary vortices are potential point vortices located at the center of vorticity. In other words, actual experimental onset of oscillation may be delayed by the primary vortices not being as coherent and strong as those modeled.

The envelope also shows a rapid decrease in the experimental envelope of Arena and Nelson at an angle of attack of 36 degrees due to vortex breakdown. The present computational effort as well as the "rocksim" effort made by Arena[49] will not predict the decrease in the amplitude because vortex breakdown is not modeled. This is regardless of the bias in the computational efforts.

The case of a delta wing at 15 degrees angle of attack is demonstrated for sake of qualitative comparison with experimental data. The experimental data is taken at an angle of attack of 30 degrees; however, the steady state amplitude of oscillation is close.
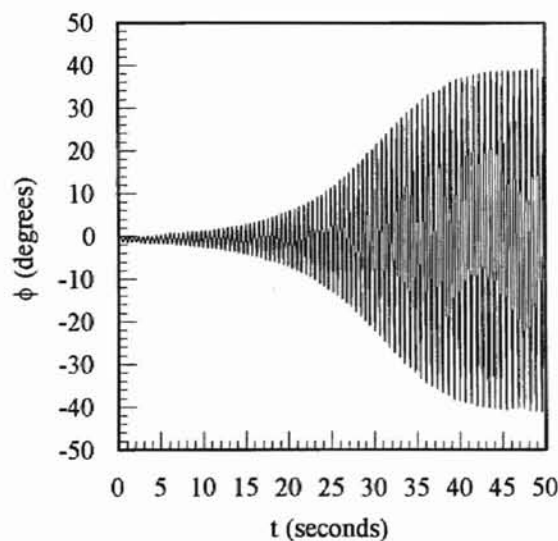


Figure 4.7 Experimental Wing Rock Time History

Investigation has shown that the model predicts a true limit cycle oscillation. The converged wing rock amplitude will be the same regardless of the initial roll angle. Figure 4.7 shows the experimental wing rock time history for the roll angle amplitude. Given a small disturbance at t=0, the wing rock oscillation builds to steady state. The steady state amplitude of the motion is about 41 degrees in the experimental case.

Figure 4.8 shows the computational wing rock time history for the rock angle amplitude. The inviscid model predicts that the steady state limit cycle amplitude to be about 46 degrees.

The fundamental parameters of lateral and normal vortex position and primary vortex strength were compared during a cycle of steady state oscillation. Figure 4.9 shows the comparison of the experimental and computational dynamic lateral vortex locations. The variations reveal a slight hysteresis in the lateral position over the majority of the range of the roll angle traversed. Experimental data from Arena for an 80 degree delta
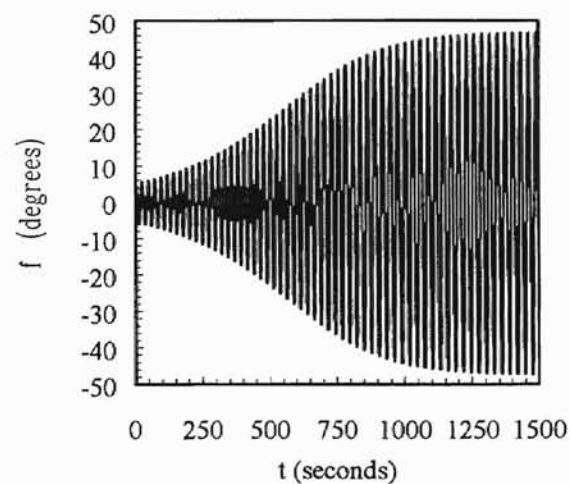


Figure 4.8   Computational Wing Rock Time
History
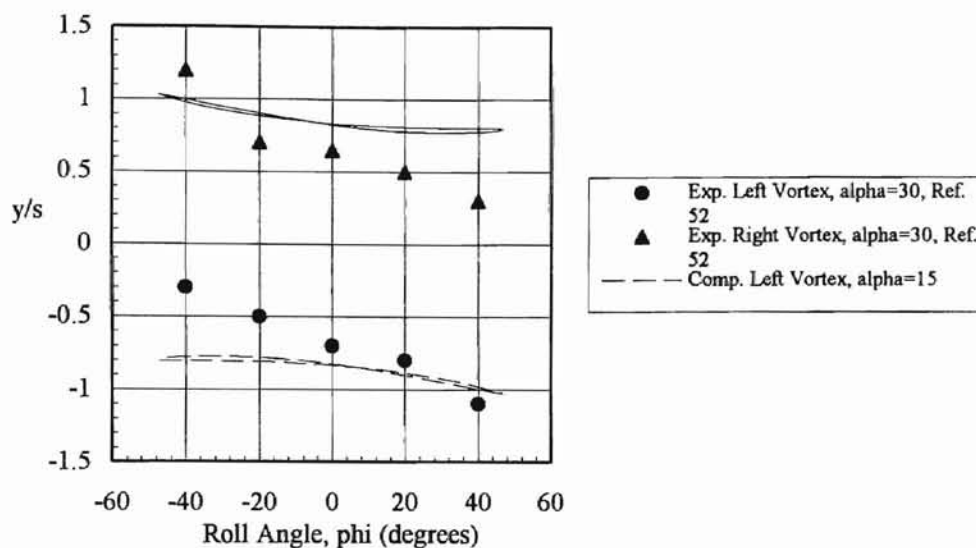
Figure 4.9 Dynamic Lateral Vortex Position

wing is also shown in Figure 4.9 The computational data is about the same order of magnitude as the experimental data. The curves are similar to the data obtained from Arena and Nelson's conformal mapping model[49] at an angle of attack at 20 degrees. A direct quantitative comparison with the conformal data cannot be made due to the present model having numerical instabilities at extreme roll angles. The predicted steady state amplitude of oscillation is about 80° as was shown in the plot of wing rock envelope. The large amplitudes lead to numerical instability due to the interference of singularity solutions between the wing panels and the primary potential vortices at 90° and -90° of roll angle.

The normal variation in position of vortices for a cycle of steady state oscillation exhibits hysteresis also. Normal variation is shown in Figure 4.11 The hysteresis for the 15 degree case is not as large as it is for the conformal model at an angle of attack of 20 degrees.
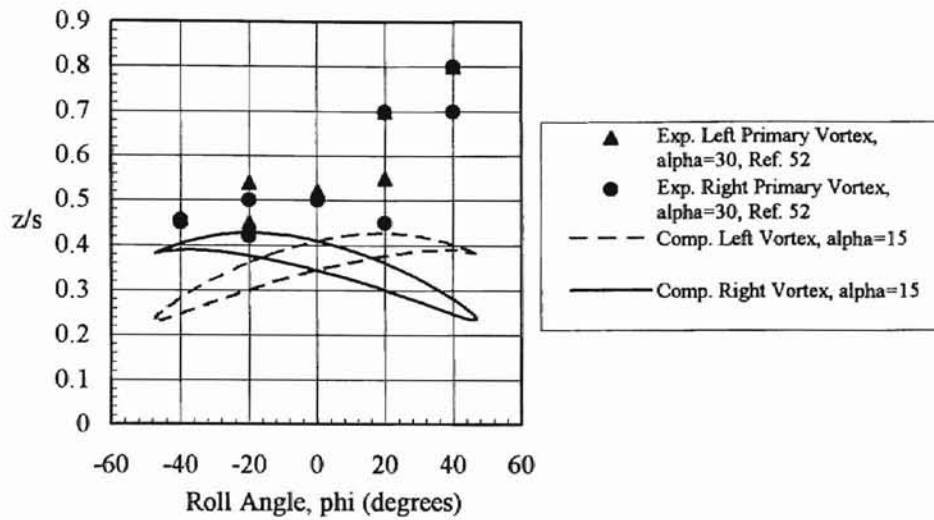
Figure 4.11  Dynamic Normal Vortex Position

The largest amount of hysteresis was found in the plot of vortex strength for a steady state cycle. The hysteresis was about 12% of the semi span at -20° and 20° of roll for the left and right vortices respectively. As the wing traversed positive roll angles, the hysteresis occurs in the right vortex. At the same time hysteresis diminishes in the left
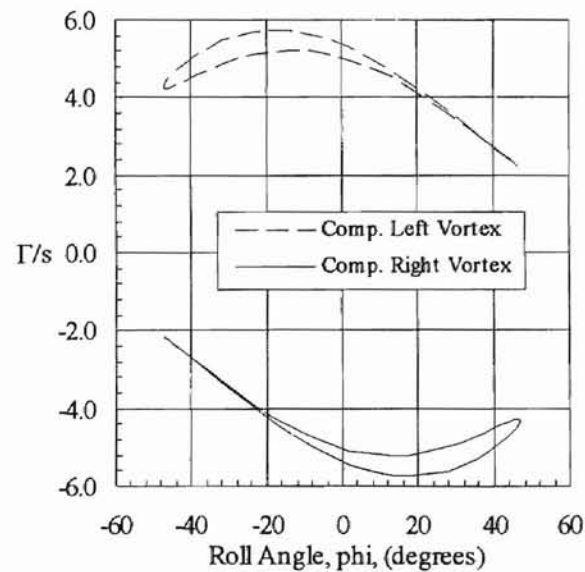


Figure 4.10  Dynamic Variation of Vortex Strength

vortex. The vice versa condition exists also. As the wing traverses negative roll angles, the hysteresis is seen in the left vortex. The hysteresis in the right vortex decreases. No experimental data could be obtained for comparison of primary vortex strengths; however, the general shape of the curves matches that in the conformal mapping study although the order of magnitude between the two studies is different. This difference cannot be easily explained away by differences in angle of attack.

These three characteristics all combine to provide a roll moment hysteresis. A plot of roll moment versus bank angle is shown in Figure 4.13. The dominance of the hysteresis in the normal position and strength of the primary vortices can be seen in counter clockwise traversed lobes at the extent of the roll travel. The roll moment for the experimental case characteristically has three loops to the hysteresis. As bank angle is decreasing, the middle loop is traversed in a counter-clockwise direction. This loop essentially is adding energy to the system. As roll passes through an angle of -25 degrees, the direction of the hysteresis loop reverses. This reversal provides damping, and the net contribution of the outer lobes is a positive roll moment at negative roll angles and a negative roll moment at positive roll angles. The reason why wing rock is limit cycle oscillation at all due to the fact that the outer damping lobes naturally balance the inner loop. The damping counteracts the energy added in the inner loop. If the outer lobes are too small, the oscillation will diverge. If the outer lobes are just slightly larger than the inner loop, the system is stable. So, two characteristics of roll moment must be present to have the wing rock limit cycle oscillation. Hysteresis must be present in the roll moment and the total areas of the hysteresis must be equal.

The computational hysteresis in Figure 4.13 shows the same characteristics as the experimental hysteresis. The computational hysteresis has balanced loops just as the
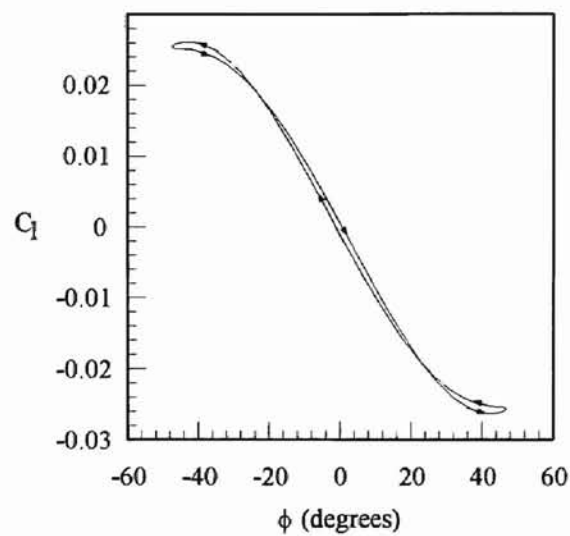


Figure 4.12    Computational Roll Moment Hysteresis versus Roll Angle for a  Steady State Cycle of Wing Rock
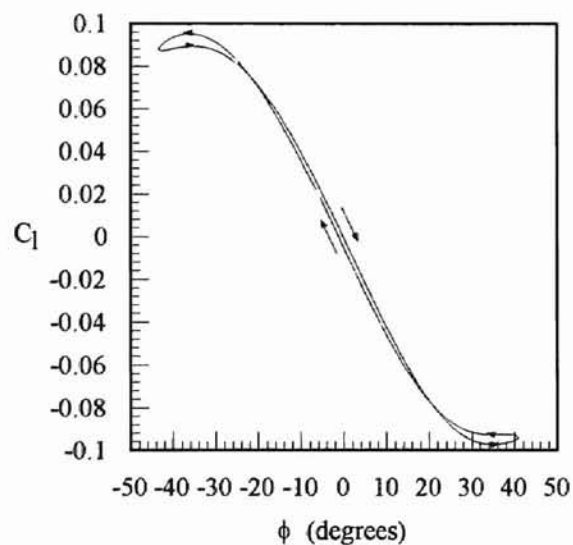


Figure 4.13    Experimental Roll Moment Hysteresis versus Roll Angle for a Steady State Cycle of Wing Rock

experimental case. The difference lies in the size of the inner loop; it is slightly larger. By being slightly larger, the inner loop of the inviscid model is adding more energy to the system. Therefore, the damping lobes must be larger to maintain steady state. As the plots show, the damping lobes are elongated to compensate for the increase in energy. With the model capturing the wing rock phenomenon qualitatively, the model can be used within its own limitations confidently. Consequently, techniques now can be explored in order to suppress the wing rock oscillation.

4.3  Static Vortex Flap Actuation

Since by observation the characteristics of the flowfield are dependent upon the boundary condition at the separation points, a control methodology was developed based on a vortex flap. A vortex flap modifies the boundary condition of the separation point by actually moving the leading edge. Since the model was developed using a conical assumption, flap must also be conical along the entire leading edge. The implementation using the panel method is show in Figure 4.14. The bevel of the delta wing is rotated about its lower corner while the connecting panel stretches to close the shape of the delta wing body. This is meant to be representative of a leading edge flap deflected. The
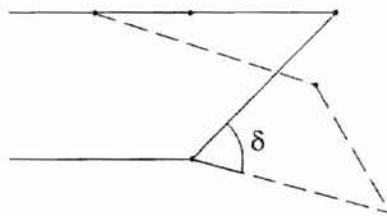
Figure 4.14  Leading Edge Vortex Flap Geometry

vortex flap on each leading edge is constrained to rotate downward only. Due to interference of the singularity panels, a maximum flap angle of 70 degrees was not exceeded.
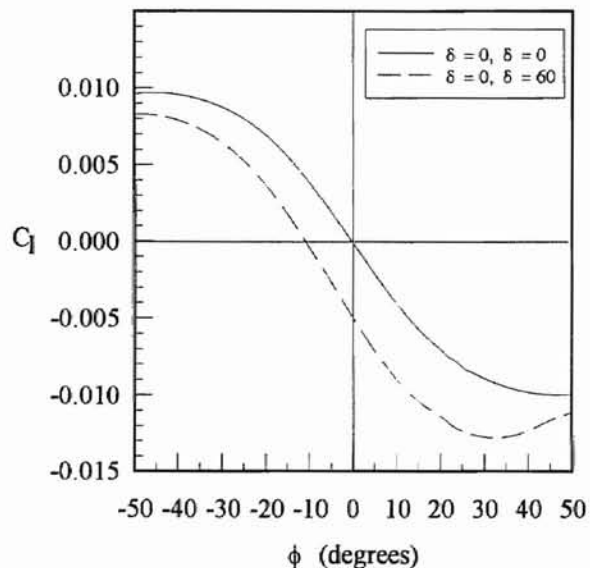


Figure 4.15  Static Roll Moment Versus Roll
Angle for Two Flap Angle
Combinations

To determine the exact effect of the leading edge vortex flaps, several test cases were run while varying each vortex flap independently. A case showing the static change in roll moment as the right flap is actuated is seen in Figure 4.15. As the right flap is deflected and the left flap is held at zero flap deflection, the sectional roll moment curve shifts down and to the left. Similarly, when the left flap is deflected while the right flap is held constant, the roll moment curve shifts up and to the right. By actuating the flap on a particular side, the roll moment decreases in the direction of the flap. Given a wing that is free to roll, the actuated flap makes the wing roll in the opposite direction of the lowered flap.

The change in roll moment caused by a actuated flap is due to a combination of the locations and strengths of the primary vortices changing. The variation of the lateral position of the primary vortices with roll angle and flap defection is shown in Figure 4.16. The flap deflection for each side affects the lateral location the most when that side of the
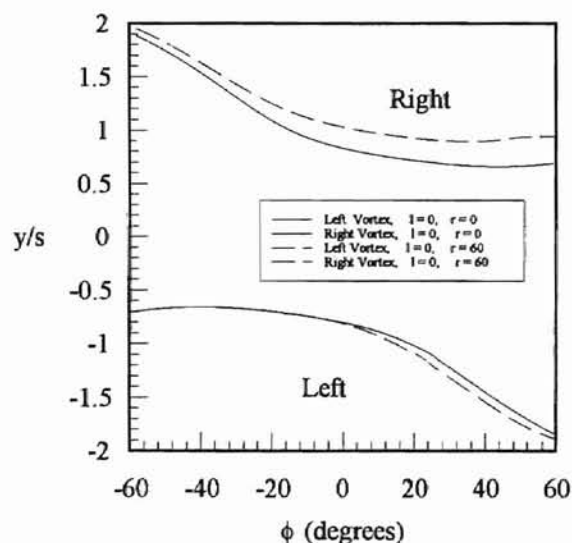


Figure 4.16   Lateral Vortex Position Variation
with Flap deflection

wing is down. For example, for a right flap deflection, the greatest affect is seen at positive roll angles. In looking at the normal position versus roll angle plot of Figure 4.17 Normal Vortex Position Variation, the primary vortices are shifted down as the right flap is deflected for the corresponding side. These characteristics of the flap deflections indicate that modifying the angle at which the flow leaves the leading edges has potential in controlling leading edge vortex flows and specifically in eliminating wing rock.
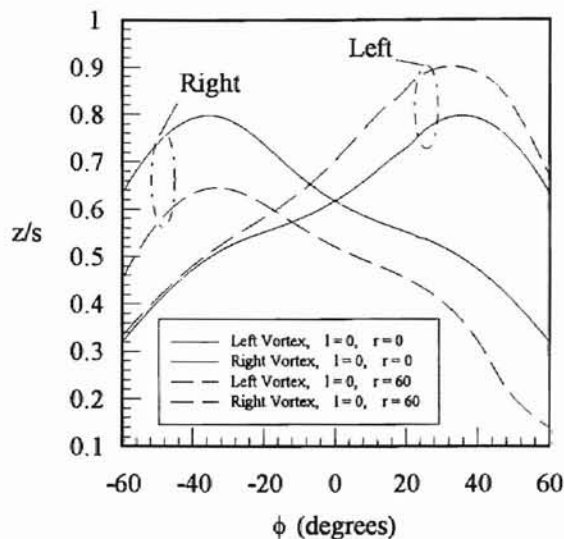
Figure 4.17 Normal Vortex Position Variation
with flap deflections and roll angle

Comparison with steady state vortex slap investigation made by Rao in 1978 shows that for several vortex flap configurations, the current study performs within the limited range of the model. The data agrees well both qualitatively as well as quantitatively. The normal force coefficient versus an angle of attack range from 0 to 32 degrees increases almost linearly from 0 to 1.7.

In Figure 4.18, when compared to a number of flap configurations studied by Rao[19] which were deflected by 30 degrees, this study's normal force accurately predicts the normal force generated on delta wing. The data splits the variance of the various flap designs presented by Rao while the variance increases with angle of attack. Wing rock data lies 18% below Rao's design with the highest data and 18% above the design with the lowest normal force at an angle of attack of 24 degrees.

These comparisons show that the magnitude of the normal force coefficient is correct for the 30 degree flap deflection case. The combination of primary vortex strength

and position is reasonable even under the conditions of the limiting assumptions. Major

assumptions are

- Inviscid flow

- The center of vorticity assumed to be concentrated at single point.

- The vorticity in the flow field was modeled by a point vortex

- The feeding sheet is assumed linear

- No vortex breakdown on the wing.


As the flap deflection increases the current study over-predicts the normal force

coefficient data as show in Figure 4.19. The over-prediction could be due to a number of

factors. The primary vortex strength per degree of flap deflection may be incorrect for

larger flap deflections. The location of the primary vortices themselves may be incorrect
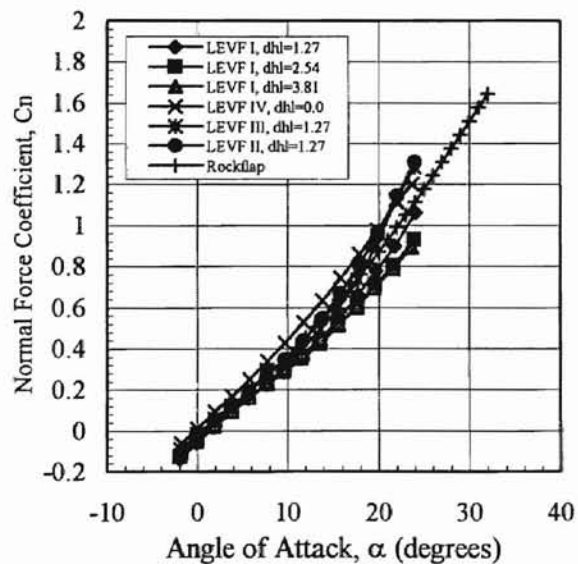


Figure 4.18  Normal Force with $\delta$=30.0
degrees
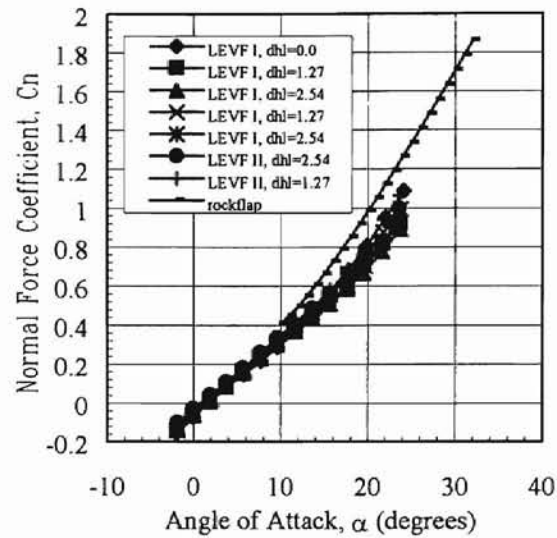
Figure 4.19 Normal Force with δ=45.0 degrees

due to amalgamating all the vorticity at the center of vorticity and modeling it with a point vortex. Furthermore, the feeding sheet panel on which a "zero-force" condition is enforced is assumed linear may not be truly linear.

## 4.4   Dynamic Vortex Flap Actuation and Control

Using an active control scheme, the vortex flaps were implemented with a derivative feedback loop into the single degree of freedom model. When the wing has a positive roll rate, the right flap is deflected by a proportion of the roll rate. When the wing has a negative roll rate the left flap is deflected by a proportion of the roll rate. The control laws are as follows:

$$\delta_r = K \cdot \dot{\phi} \quad \text{if } \dot{\phi} > 0$$
$$\delta_l = K \cdot \dot{\phi} \quad \text{if } \dot{\phi} < 0$$

where K is the gain on the feedback loop. For this case, $\alpha = 15°$, $\Lambda = 80°$, the gain is set to a value of 1.5 (K = 1.5) The flaps are limited to a maximum deflection of 70° to prevent interference of the singularity solutions.

Promising effects can be seen immediately by implementing this feedback loop. Feedback control decreases the amplitude by about half within two cycles of the control laws being turned on. In Figure 4.20, the amplitude decreases from 47 degrees to about 20 degrees within two cycles of the control being turned on. The time to half amplitude is about 50 time steps.
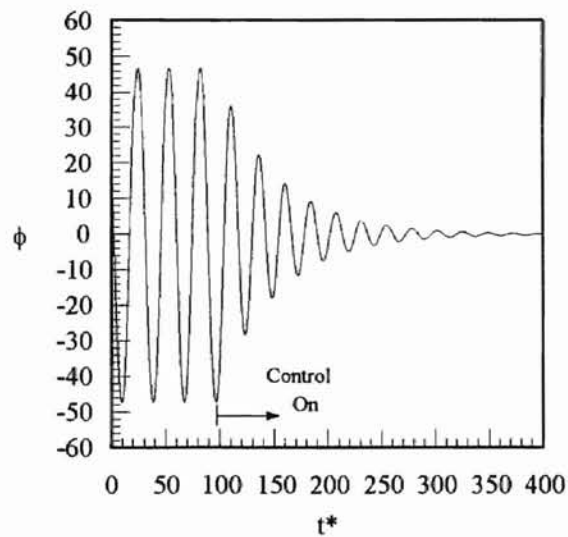
Figure 4.20 Wing Rock Suppression
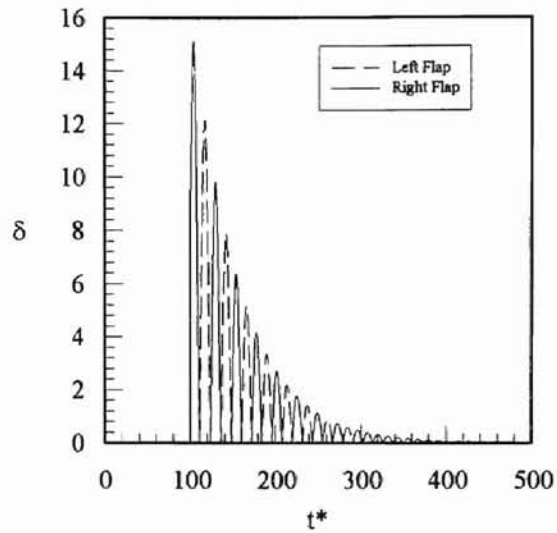
Figure 4.21  Flap Deflection History During
Control

The flap deflection history is shown for the same control cycle in Figure 4.21. This control method is nonlinear since the flaps are not allowed to rotate up. The maximum deflection of the flaps occurs when the control is first turned on. The flap deflections quickly diminish revealing that the roll rate is indeed being affected. The total
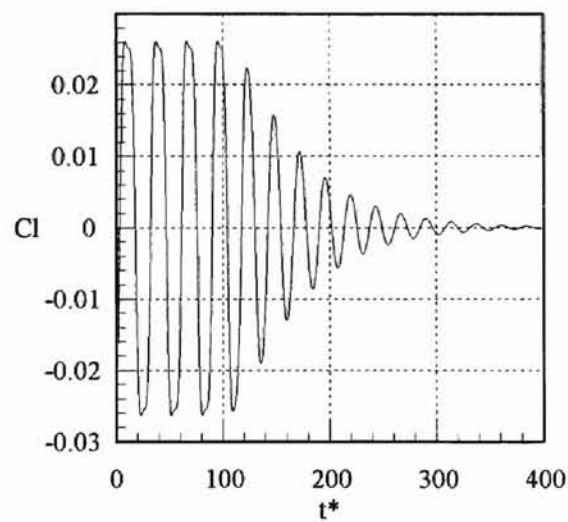


Figure 4.22  Roll Moment Time History During
Control

computational time needed to investigate a control methodology, is about 5 hours on a time shared IBM RS6000 workstation. This time includes letting wing rock build to steady state about a total of 80 cycles and then damping the oscillation by 90% in about 8 cycles. A total of 50,000 time steps were needed to resolve the build up and damping of the wing rock oscillation.

Observation of the parameters that combine to drive the wing rock oscillation demonstrates the ability to not only control the combination of the parameters, but the individual parameters as well. Each parameter, y/s, z/s, γ/s, is controlled and converges to a finite value. As steady state damped conditions are reached, the fluctuations of the lateral and normal positions and vortex strengths are not merely canceling each other, but the deviations of the values are diminishing. Significant damping is accomplished within 2 cycles of control being turned on.

In Figure 4.23 the characteristic steady state oscillation is shown along with the spiraling lateral vortex position after control was turned on. The lateral vortex position on
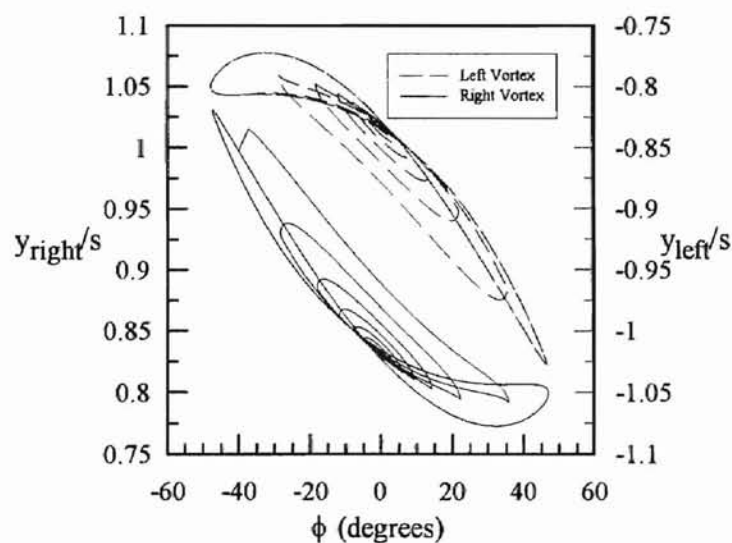


Figure 4.23 Dynamic Lateral Vortex Position during Control
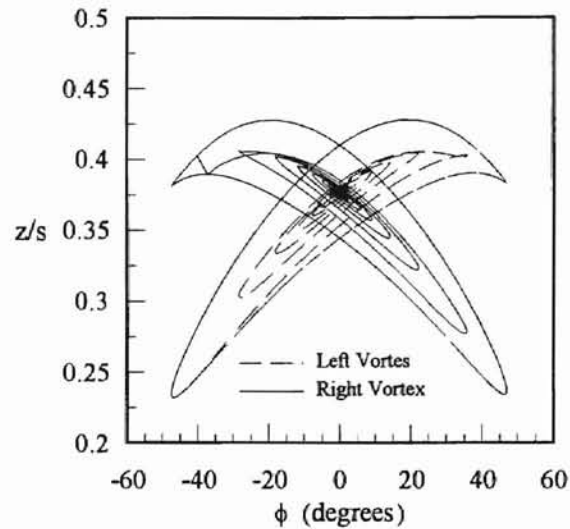
Figure 4.24 Dynamic Normal Vortex Position
during Control

each side oscillates about the point $\phi$=0., $|y/s|$ = 0.825 until finally converging after about

six cycles.

Figure 4.24 shows the left vortex departing from the steady state loop better. The

normal position spirals counterclockwise until converging at $z/s$=0.375. The right vortex

is similar except that the spiral motion occurs in the clockwise direction.

The control algorithm affects the vortex strength immediately by increasing the

strength in the respective directions. The flaps gradually diminish the strength until

converging upon a value of $|\gamma/s|$=5.4.

The exact effect of the flap is best seen in Figure 4.26. During the last cycle of the wing rock oscillation before control is turned on, the cycle still exhibits the three major loops as seen previously. When control is turned on, the roll moment decreases in a counter clockwise spiral toward zero moment. The counter clockwise spiral denotes a stable dynamic system. The roll moment decreases as the roll angle decreases until the motion is damped out completely. Thus, a promising technique to alleviate wing rock is one that is able to dynamically move the points of separation with respect to the main wing.
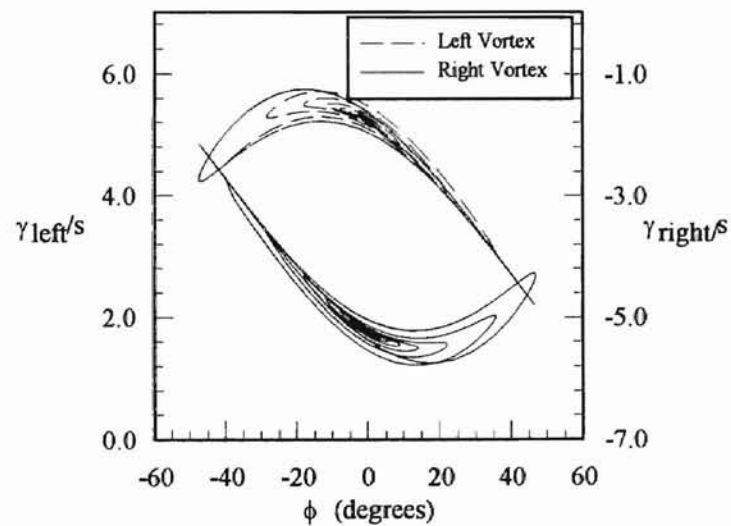
Figure 4.25 Dynamic Vortex Strength during Control
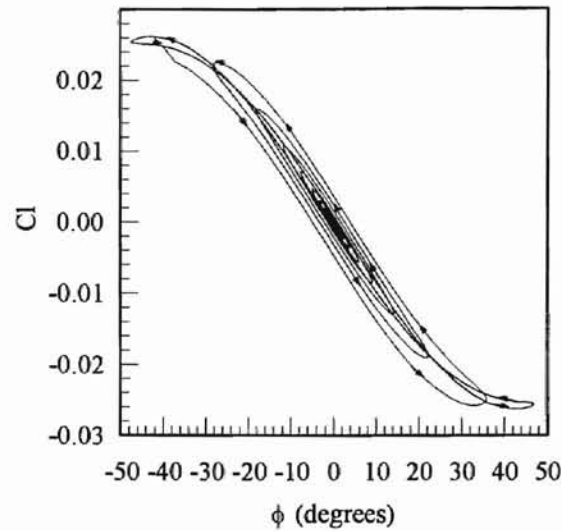
Figure 4.26   Roll Moment versus Roll Angle
Stability Curve

## 4.5 Projected Control Methodologies

A panel method was used so that arbitrary geometries and control techniques could be implemented to investigate the alleviation of wing rock. Spanwise blowing and vortex control flaps are two methods proposed by previous investigators to control the oscillation. The hysteresis of the vortices' location and strength has been controlled by a leading edge flap in this investigation by moving the separation point with respect to the wing enough to control the location of the vortices. Arena[49] documents that a distinctive characteristic of vortex behavior on delta wing during wing rock is that hysteresis in position is confined to the direction normal to the surface of the wing. This suggests that wing rock will be able to be controlled through blowing on the upper surface of the wing since blowing is able to move the separation point of the emanating shear layer. This is in fact the conclusion at which Wong[36] arrives by implementing a dynamic feedback system

alone. Wong is able to attenuate the wing rock motion significantly. This does not prove that the source of wing rock is eliminated, however. By approaching the problem from a coupling of the aerodynamics with the vehicle dynamics, a better knowledge of the physics is attained, and therefore, the physics can be exploited to its fullest extent.

# CHAPTER 5

## CONCLUSIONS AND RECOMMENDATIONS

### 5.1 Conclusions

In the investigation of separated vortical flows, this effort has demonstrated the flexibility of an inviscid panel method to capture the primary characteristics of a dynamic separated vortical flow field quickly. Specifically, this study addressed a solution to a nonlinear flow field / vehicle dynamic instability known as wing rock. Several aspects of the model make it useful in primary parameter identification as well as in an iterative search for control solutions to separated vortical flows. The aspects which are important are the simplifying assumptions, ease of modeling a given geometry and flow field, and the execution time required to predict a dynamic solution.

The simplifying assumptions of the problem definition were balanced against the ease of geometry discretization, flow field accuracy, and type of information desired. Since primary characteristics of the flow field were desired, flow field accuracy was not as important as the ease of modeling the geometry and the rapidity of the solution. Simplifying assumptions such as an inviscid, conical flow field allowed the problem geometry to be reduced to 2D and flow field to be reduced to a quasi-3D scenario.

Additionally, the panel method used in this study allowed the 2D geometry to be easily modeled. The leading edges of the delta wing were modeled with a 45 degree

corner so that separation could be accurately placed at the leading edges. Wing thickness could also be modeled as long as the singularity solutions on each panel were not close to each other. The gridding of the geometry was accomplished quickly so that the geometry could be re-paneled at every time step. During the dynamic solution, any geometry motion such as the flaps was handled by re-paneling at every time step.

The flow field solution was determined by using singularity solutions of the inviscid flow field on each panel of the geometry. Given the linear nature of the steady state solution, the static singularity solutions were used in matrix form to determine the static portion of the solution. The dynamic piece of the solution was then added to the static solution to determine the total solution. The dynamic piece of the total solution was potentially a very time consuming, as the potential of the flow field changes with time and must be integrated from the far field where the flow field is not changing.

Validation of the solution for a static delta wing showed good agreement with experimental data available. Since the inviscid model assumes that the viscous forces are negligible, closer agreement theoretically could be obtained by using experimental data obtained at increasingly higher Reynolds numbers in the turbulent flow regime. The present comparisons are to data from Arena at a Reynolds number of 400,000. Excellent agreement was obtained for the static sectional roll moment for roll angles between -22 degrees and 22 degrees.

The dynamic validation captured the qualitative characteristics of the roll moment hysteresis formed when the hysteresis of primary vortex position and strength combine. The three major loops which form the hysteresis in the experimental data were captured in the computational data as well.

Time of execution for the whole dynamic model was reasonable. For 50,000 time steps, an actual time of 5 hours was needed on a timeshared RS6000 320H workstation. Other platforms were able to perform better. A timeshared RS6000 530 workstation needed 2.5 hours to complete the task while a Harris Nighthawk 5800 workstation needed 1.75 hours. The actual program include disk input/output to a file; so a data recording scheme which did not need disk i/o would make the total time slightly faster.

These total times make iteration on solutions tolerable and feasible. Within a few hours, dynamic characteristics can be obtained to help determine the fundamental flow field dependencies involved. Once the primary dependencies are identified and the primary characteristics captured, the a control solution can be systematically investigated. Different geometries can be modeled quickly using panels and singularity solutions while control laws can be developed for each geometry. For the wing rock case, the limit cycle oscillations could be controlled by actively controlling the roll moment proportionally to the magnitude and direction of the roll rate. A limit cycle oscillation could be completely damped out in 10 cycles with 90 % damping within 8 cycles.

5.2 Recommendations

During the course of this investigation, the simplifying assumptions, method of solution, and results have led to several recommendations.

1. During the development of the inviscid model a topic of academic interest arose. The selection of singularity solutions should be arbitrary since the steady state problem is linear and each singularity solution by itself satisfies Laplace's equation.. However, the selection and distribution of the singularities was important in this model. Certain combinations of singularities and distributions led ill-conditioned matrices which proved to be either difficult to solve or take longer to solve. Guidelines for selection of combinations of singularities and distributions could be investigated.

2. Additional methods of physically controlling roll moment such as blowing could be investigated for use with panel methods. Blowing methods have been demonstrated in experimental efforts. Placing these methods in the context of the actual aerodynamics namely their affect on rolling moment hysteresis in separated leading edge vortical flows is another area of potential investigation. Perhaps higher order "blowing panels" or blowing regions which specify normal velocity gradients could be developed.

3. Once blowing panels are developed, the effect of blowing on the separation angle of the primary vortex and location of the primary vortex core. Modifying the local angle of separation may not have a great affect on the location of the primary vortex core. How much mass flow would it take to modify the core location?

4. Using any method, can hysteresis in roll moment be controlled with vortex strength instead of vortex position? Can vortex strength be dynamically changed without changing position of the vortex or velocity of the free stream?

5. In this model, the "no force" condition for the wake is satisfied on the linear feeding sheet. The feeding sheet could be discretized with more panels and the no force condition satisfied on each panel for more accuracy.

# REFERENCES

[1] Fisher, D. F. and Del Frate, J. H., "In-Flight Flow Visualization Characteristics of the NASA F-18 High Alpha Research Vehicle at High Angles of Attack", SAE Technical Paper Series No. 892222, September 1989.

[2] Gordnier, R. E., and Visbal, M. R., "Numerical Simulation of Delta Wing Roll", AIAA 93-0554, January 1993.

[3] Chaderjian, N. M., "Navier-Stokes Prediction of Large-Amplitude Delta-Wing Roll Oscillations Characterizing Wing Rock", AIAA 92-4428-CP, August 1992.

[4] Brown, C. E., and Michael Jr., W. H., "On Slender Delta Wing with Leading Edge Separation", NACA TN-3430, April 1955.

[5] Mangler, K. W., and Smith, J. H. B., "Calculation of the Flow Past Slender Delta Wings with Leading Edge Separation", RAE Report No. Aero. 2593, May 1957.

[6] Konstadinopoulos, P., et al., "A Vortex-Lattice Method for General, Unsteady Aerodynamics", Journal of Aircraft, Vol. 22, No. 1, January 1985.

[7] Arena Jr., A. S., and Nelson, R. C., "Unsteady Surface Pressure Measurement on a Slender Delta Wing Undergoing Limit Cycle Wing Rock", AIAA 91-0434, January 1991.

[8] Arena, Jr., A. S., Nelson, R. C., and Schiff, L. B., "An Experimental Study of the Nonlinear Dynamic Phenomenon Known as Wing Rock", AIAA 90-2812, August 1990.

[9] Roberts, S. D., and Arena, A. S., "An Inviscid Model for Evaluating Wing Rock Suppression Methodologies", AIAA-94-0808, January 1994.

[10] Nelson, R. C., "Unsteady Aerodynamics of Slender Wings", AGARD-R-776, March 1991.

[11] Herbst, W. B., "Future Fighter Technologies", Journal of Aircraft, Vol 17., Vol. 4, August 1980.

[12] Lang, J. O., and Francis, M. S., "Unsteady Aerodynamics-Fundamentals and Applications to Aircraft Dynamics," AGARD-CP-386, April 1985.

92

13    Ashley, H., "On the Feasibility of Low-Speed Aircraft Maneuver Involving Extreme Angles of Attack", Journal of Fluids and Structures, 1:319-335, 1987.

14    Hsu, C. H., and Lan, C. E., "Theory of Wing Rock", Journal of Aircraft, Vol. 22, No. 10, October 1985.

15    Beecham, L. J., and Titchener, I. M., "Some Notes on an Approximate Solution for the Free Oscillation Characteristics of Non-Linear Systems Typified by $\ddot{x} + F(\dot{x}, x) = 0$", British A.R.C.R. and M 3651, 1969.

16    Elzebda, J. M., Hayfeh, A. H., and Mook, D. T., "Developement of an Analytical Model of Wing Rock for Slender Delta Wings", Journal of Aircraft, Vol. 26, No. 8, August 1989.

17    Nayfeh, A. H., Elzebda, J. M., and Mook, D. T., "Analytical Study of the Subsonic Wing-Rock Phenomenon for Slender Delta Wings", Vol. 26, No. 9, Septermber 1989.

18    Luo, J., and Lan, C. E., "Control of Wing-Rock Motion of Slender Delta Wings", Journal of Guidance, Control, and Dynamics, Vol. 16, No. 2, March-April 1993.

19    Rao, D. M., "Investigation of Delta Wing Leading Edge Devices", Journal of Aircraft, Vol. 18, No. 3, March 1981.

20    Robins, A. W., and Carlson, H. W., "High-Performance Wings With Significant Leading-Edge Thrust at Supersonic Speeds", Journal of Aircraft, Vol. 17, June 1980.

21    Marchman, III, J. F., "The Aerodynamics of Inverted Leading Edge Flaps of Delta Wings", AIAA-81-0356, AIAA 19th Aerospace Sciences Meeting, January 1981.

22    Marchman, III, J. F., "Effectiveness of Leading-Edge Vortex Flaps on 60 and 75 Degree Delta Wings", Journal of Aircraft, Vol. 18, No. 4, April 1981.

23    Grantz, A. C., and Marchman, III, J. F., "Trailing Edge Flap Influence on Leading Edge Vortex Flap Aerodynamics", Journal of Aircraft, Vol. 20, No. 2, February 1983.

24    Murman, E. M., et al., "Comparison of Computation and Experimental Data for Leading Edge Vortices -- Effects of Yaw and Vortex Flaps", AIAA-86-0439, AIAA 24th Aerospace Sciences Meeting, Revo, NV., January 1986.

25    Powell, K. G, and Murman, E. M., et al., "A Comparison of Experimental and Numerical Results for Delta Wings with Vortex Flaps", Journal of Aircraft, Vol. 25, No. 5, May 1988.

[26] Murman, E. M., and Rizzi, A., "Applications of Euler Equations to Shap Edge Delta Wings With Leading Edge Vortices", AGARD -CP-412.

[27] Ng, T. T., and Malcolm, G. N., "Forebody Vortex Control Using Small, Rotatable Strakes", Journal of Aircraft, Vol. 29, No. 4, July-August 1992.

[28] Synolakis, C. E., et al., "Passive Control of Delta Wing Rock", Journal of Aircraft, Vol. 30, No. 1, January-February 1993.

[29] Walton, J., and Katz, J., "Reduction of Wing Rock Amplitudes Using Leading-Edge Vortex Manipulations", AIAA 92-0279, January 1992

[30] Ng, T. T., et al., "Effect of Leeward Flow Dividers on the Wing rock of a Delta Wing", AIAA 93-3492-CP

[31] Klute, S. M., et al., "Flow Control over Delta Wings at High Angles of Attack", AIAA 93-3494-CP

[32] Syverud, E., et al., "Aerodyanmic Characteristics of a Delta Wing with a Body-Hinged Leading Edge Extension", AIAA-93-3446-CP.

[33] Rinoie, K., and Stollery, J. L., "Experimental Studies of Vortex Flaps and Vortex Plates", Journal of Aircraft, Vol. 31, No. 2, March-April 1994.

[34] Campbell, J. F., "Augmentation of Vortex Lift by Spanwise Blowing", Journal of Aircraft, Vol. 13, No. 9, September 1976.

[35] Celik, Z. Z., and Roberts, L., and Wood, N. J., "An Investigation of Asymmetric Vortical Flows over Delta Wings with Tangential Leading-Edge Blowing at High Angles of Attack", AIAA 90-103, January 1990.

[36] Wong, G. S., "Experiments in the Control of Wing Rock at High Angle of Attack Using Tangential Leading Edge Blowing", Ph.D. Thesis, Stanford University, June 1992.

[37] Suarez, C. J., et al., "Forebody Vortex Control for Suppressing Wing Rock on a Highly-Swept Wing Configuration", AIAA 92-2716-CP.

[38] Greenwell, D. I., and Wood, N. J., "Control of Asymmetry Vortical Flows", AIAA 91-3272-CP.

[39] Bean, et al., "Vortex Control Technique for the Attenuation of Fin Buffet", Journal of Aircraft, Vol. 30. No. 6, November-December 1993.

[40] Crowther, W. J., and Wood, N. J., "Tangentail Forebody Blowing-Yaw Control at High Alpha", AIAA 93-3406-CP

[41] Kramer, B. R, et al., "Forebody Vortex Control with Jet and Slot Blowing on an F/A-18", AIAA93-3449-CP.

[42] Celik, Z. Z., Pedreiro, N., and Roberts, L., "The Control of Wing Rock by Forebody Blowing", AIAA 93-3685.

[43] Ng, T. T., et al., "Forebody Vortex Control for Wing Rock Suppression", Journal of Aircraft, Vol. 31, No. 2, March-April 1994.

[44] Wong, G. S., et al., "Active Control of Wing Rock Using Tangential Leading Edge Blowing", Journal of Aircraft, Vol. 31, No. 3, May-June 1994.

[45] Arena, Jr., A. S., Nelson, R. C., and Schiff, L. B., "Lateral Control at High Angles of Attack Using Pneumatic Blowing Through a Chined Forebody", AIAA 93-3624.

[46] Gittner, N. M., and Chokani, N., "Effects of Nozzle Exit Geometry on Forebody Vortex Control Using Blowing", Journal of Aircraft, Vol. 31, No. 3, May-June 1994

[47] Legendre, R., "Ecoulment au voisinage de la pointe avant d'une aile a forte fleche aux incidences moyennes", La Recherche Aeronautique (ONERA), No. 30, Nov.-Dec., 1952, pp. 3-8, No. 31, Jan.- Feb.., 1953, pp. 3-6

[48] Visser, K. D., "An Experimental Analysis of Critical Factors Involved in the Breakdown Process of Leading Edge Vortex Flows", Ph.D. Dissertation, University of Notre Dame, April, 1991.

[49] Arena Jr., A. S., "An Experimental and Computational Investigation of Slender Wings Undergoing Wing Rock", Ph.D. Dissertation, University of Notre Dame, April 1992.

[50] Arena Jr., A. S., and Nelson, R. C., "A Discrete Vortex Model for Predicting Wing Rock of Slender Wings", AIAA 92-4497, August 1992.

[51] Katz, J., and Plotkin, A., *Low-Speed Aerodynamics: From Wing Theory to Panel Methods*, McGraw Hill, Inc., 1990

[52] Hummel, D., "On the Vortex Formation over a Slender Wing at Large Angles of Incidence", AGARD CP-247, 1978.

[53] Nguyen, L. T., Yip, L., and Chambers, J. R., "Self-Induced Wing Rock of Slender Delta Wings", AIAA Paper 81-1883, August 1981.

[54] Levin, D., and Katz, J., "Dynamic Load Measurements with Delta Wings Undergoing Self-Induced Roll Oscillations", Journal of Aircraft, Vol. 21, No. 1, January 1984.

## ROCKFLAP SIMULATION CODE

ROCKFLAP: Leading Edge Vortex Flow Model with Leading Edge Vortex Flaps.

```
program rockflap

real ep(200,2), ept(200,2), pt1(200,2), pt2(200,2),pot(200,2)
real co(200,2), a(200,200), b(200,200), g(200),pinft,pinfb
real th(200),pi,dl(200),vpos(2,2),vposo(2,2),gam(2,3),velt(200)
real phix(200),dli,cp(200),dgamdt(2),dpotdt(200),r(200),bet(200)
real phidot(2),phi(2),aa(200,200),uv(200),wv(200),vn(200)
real dens,cr,inertia,inrf,kgain,dphi

pi=4.*atan(1.)

open(8,file='cps20ae.dat')
open(9,file='pos20ae.dat')

m = 40
c   write(*,*)'enter angle of attack (deg.)'
c   read(*,*)alphad
        alphad=20.0
c   write(*,*)'input crf '
c   read(*,*)crf
        crf=1.0
c   write(*,*)'enter initial roll angle (deg.) '
c   read(*,*)phid
        phid=5.0
    swd=80
    inrf=3.0
c   write(*,*)'enter left flap angle (deg.) '
c   read(*,*)deltld
    deltld=0.
c   write(*,*)'enter right flap angle (deg.) '
c   read(*,*)deltrd
    deltrd=0.
    iend=50000
    icntrl=35000
    kgain=1.5
c        do jk=-50,50
c        phid=jk*1.0

    alpha = alphad*pi/180.
    phi(1) = phid*pi/180.
    rho = pi/2. + phi(1)
    eps = pi/2. - swd*pi/180.
```

```
    deltl = deltld*pi/180.
    deltr = deltrd*pi/180.

    xc = .66
    dens = 0.0023
    cr = 1.385
    inertia = 0.00083 / inrf vpos(1,1)=-0.738
    vpos(1,2)=0.626
    vpos(2,1)=0.738
    vpos(2,2)=0.626

    dt=0.05
    n = m + 4
    phidot(1) = 0.0
    dgamdt(1)=0.
    dgamdt(2)=0.

c =======================================================

    idyn = 0
    istep = 0

 5 continue


c  initialize [a]matrix
    do i=1,n
     do j=1,n
      a(i,j)=0.0
     end do
    end do

c  read in the panel end points

      call body(m,ept,deltl,deltr)

c  convert panelling to clockwise

    do i=1,m+1
      ep(i,1)=ept(m+1-i+1,1)
      ep(i,2)=ept(m+1-i+1,2)
    end do

c  establish coordinates of panel end points

    do i=1,m
      pt1(i,1)=ep(i,1)
      pt2(i,1)=ep(i+1,1)
      pt1(i,2)=ep(i,2)
      pt2(i,2)=ep(i+1,2)
    end do

c  find panel angles th(j) and length
```

```fortran
      tlength = 0.

      do i=1,m
        dz=pt2(i,2)-pt1(i,2)
        dx=pt2(i,1)-pt1(i,1)
        th(i)=atan2(dz,dx)
        dl(i) = sqrt(dx**2+dz**2)
             tlength = tlength + dl(i)
      end do

c   establish colocation points

      do i=1,m
        co(i,1)=(pt2(i,1)-pt1(i,1))/2.0 + pt1(i,1)
        co(i,2)=(pt2(i,2)-pt1(i,2))/2.0 + pt1(i,2)
      end do


c   establish influence coefficients

      do i=1,m
        uv(i)=0.
        wv(i)=0.
        do j=1,m

c   convert colocation point to local panel coordinates
      xt=co(i,1)-pt1(j,1)
      zt=co(i,2)-pt1(j,2)
      x2t=pt2(j,1)-pt1(j,1)
      z2t=pt2(j,2)-pt1(j,2)

      x=xt*cos(th(j))+zt*sin(th(j))
      z=-xt*sin(th(j))+zt*cos(th(j))
      x2=x2t*cos(th(j))+z2t*sin(th(j))
      z2=0.

c   find r1, r2, th1, th2
      r1=sqrt(x**2+z**2)
      r2=sqrt((x-x2)**2+z**2)

      th1=atan2(z,x)
      th2=atan2(z,x-x2)

c   compute velocity in local reference frame

      if(i.eq.j) then
        ul=0.
        wl=0.5
        ulv= 0.5
        wlv= 0.
      else
        ul=1./(2.*pi)*log(r1/r2)
        wl=1./(2.*pi)*(th2-th1)
        ulv = 1./(2.*pi)*(th2-th1)
        wlv = 1./(2.*pi)*log(r2/r1)
```

```
      end if

c  return velocity to global reference frame
   u=ul*cos(-th(j))+wl*sin(-th(j))
   w=-ul*sin(-th(j))+wl*cos(-th(j))
   uv(i) = uv(i) + ulv*cos(-th(j)) + wlv*sin(-th(j))
   wv(i) = wv(i) - ulv*sin(-th(j)) + wlv*cos(-th(j))


c  a(i,j) is the influence coefficient defined by the
c  tangency condition.  b(i,j) is the induced local
c  tangential velocity to be used in Cp calculation

   a(i,j)=-u*sin(th(i))+w*cos(th(i))
   b(i,j)=u*cos(th(i))+w*sin(th(i))

   aa(i,j) = a(i,j)

      end do
   end do


C=============================================================

 10    continue

   do i=1,m

     do j=1,m
      a(i,j) = aa(i,j)
     end do

   a(i,m+1) = -uv(i)*sin(th(i)) + wv(i)*cos(th(i))
   b(i,m+1) = uv(i)*cos(th(i)) + wv(i)*sin(th(i))


c  shed vortex influence

   xleft = co(i,1) - vpos(1,1)
   zleft = co(i,2) - vpos(1,2)
   uleft = 1.0/(2.*pi)*zleft/(xleft**2+zleft**2)
   wleft = -1.0/(2.*pi)*xleft/(xleft**2+zleft**2)

   xright = co(i,1) - vpos(2,1)
   zright = co(i,2) - vpos(2,2)
   uright = 1.0/(2.*pi)*zright/(xright**2+zright**2)
   wright = -1.0/(2.*pi)*xright/(xright**2+zright**2)

   a(i,m+2) = -uleft*sin(th(i)) + wleft*cos(th(i))
   a(i,m+3) = -uright*sin(th(i)) + wright*cos(th(i))

   b(i,m+2) = uleft*cos(th(i)) + wleft*sin(th(i))
   b(i,m+3) = uright*cos(th(i)) + wright*sin(th(i))

c  RHS
```

```
    r(i) = sqrt( co(i,1)**2 + co(i,2)**2 )
    bet(i) = atan2(co(i,2),co(i,1))

    vn(i)=-xc*phidot(1)*tan(eps)/sin(alpha)*r(i)*cos(bet(i)-th(i))

    a(i,n)=cos(rho)*sin(th(i))-sin(rho)*cos(th(i)) + vn(i)

    end do

c   KUTTA condition


    do j=1,m+3
      a(m+1,j) = b(1,j) + b(m,j)
      a(m+1,m+4) = - ( cos(rho-th(1))+cos(rho-th(m)) )
      a(m+2,j) = b(m/2,j) + b(m/2+1,j)
      a(m+2,m+4)=-( cos(rho-th(m/2))+cos(rho-th(m/2+1)) )
    end do


c   Kelvin Condition

    a(m+3,m+1) = tlength
    a(m+3,m+2)=1.0
    a(m+3,m+3)=1.0
    a(m+3,m+4)=0.

c   solve for solution vector

    call matrx(a,n,g)

    do i=1,2
     gam(i,3)=g(m+1+i)
     vposo(i,1)=vpos(i,1)
     vposo(i,2)=vpos(i,2)
    end do

    do ig=1,2
     if(idyn.eq.0)then
      dgamdt(ig) = 0.
     else
      dgamdt(ig) = ( gam(ig,3) - gam(ig,1) ) / (2.*dt)
     end if
    gam(ig,1) = gam(ig,2)
    gam(ig,2) = gam(ig,3)
    end do

c   Calculate vortex position

    rv = sqrt( vposo(1,1)**2 + vposo(1,2)**2 )
    thetv = atan2(vposo(1,2),vposo(1,1))

    call xzvel(u,w,vposo(1,1),vposo(1,2),rho,
     &   pt1,pt2,g,th,m,vposo,gam,2,1)
```

```fortran
vxg1 =  u*sin(alpha)/(xc*tan(eps))
   & -cos(alpha)*vposo(1,1)/xc - crf*(vposo(1,1)-ep(m/2+1,1))*
   & (cos(alpha)/xc + dgamdt(1)/gam(1,3))

vzg1 =  w*sin(alpha)/(xc*tan(eps))
   & -cos(alpha)*vposo(1,2)/xc - crf*(vposo(1,2)-ep(m/2+1,2))*
   & (cos(alpha)/xc + dgamdt(1)/gam(1,3))


rv = sqrt( vposo(2,1)**2 + vposo(2,2)**2 )
thetv = atan2(vposo(2,2),vposo(2,1))

call xzvel(u,w,vposo(2,1),vposo(2,2),rho,
   & pt1,pt2,g,th,m,vposo,gam,2,1)

vxg2 = u*sin(alpha)/(xc*tan(eps))
   & -cos(alpha)*vposo(2,1)/xc - crf*(vposo(2,1)-ep(m+1,1))*
   & (cos(alpha)/xc + dgamdt(2)/gam(2,3))

vzg2 = w*sin(alpha)/(xc*tan(eps))
   & -cos(alpha)*vposo(2,2)/xc - crf*(vposo(2,2)-ep(m+1,2))*
   & (cos(alpha)/xc +dgamdt(2)/gam(2,3))


vpos(1,1) = vposo(1,1) + vxg1 * dt
vpos(1,2) = vposo(1,2) + vzg1 * dt
vpos(2,1) = vposo(2,1) + vxg2 * dt
vpos(2,2) = vposo(2,2) + vzg2 * dt

v11 = vpos(1,1)
v12 = vpos(1,2)
v21 = vpos(2,1)
v22 = vpos(2,2)

if(idyn.eq.0)then

if(mod(icount,10).eq.1)write(*,*)'norm = ',tnorm
icount = icount + 1

tnorm = sqrt( (vposo(2,1)-vpos(2,1))**2
   & + (vposo(2,2)-vpos(2,2))**2 )

if(tnorm.gt.0.00001)goto 10

write(*,*)' '
write(*,*)' '
write(*,*)'Static Solution'
write(*,*)'Number of iterations = ',icount
write(*,*)vpos(1,1),vpos(1,2),g(m+2)
write(*,*)vpos(2,1),vpos(2,2),g(m+3)
write(*,*)' '

idyn = 1
```

```
      end if


c     convert source strengths into tangential velocities
c     along the airfoil surface and Cps on each panel

c     Calculate crossflow velocity at each panel

      do i=1,m
        velt(i)=0.
        do j=1,m+3
          velt(i)=velt(i)+b(i,j)*g(j)*sin(alpha)
        end do
          velt(i) = velt(i) + sin(alpha)*cos( rho - th(i) )
      end do

c     Calculate pert. potential at center of top sfc.

      dz=0.2
      pinft=0.
      do i=1,49
       x=co(3*m/4,1)
       z1=10.+(co(3*m/4,2)+0.001) - dz*float(i)
      call xzvel(u,w,x,z1,rho,pt1,pt2,g,th,m,vposo,gam,2,0)
       w1 = w*sin(alpha)
       z2=10.+(co(3*m/4,2)+0.001) - dz*float(i+1)
      call xzvel(u,w,x,z2,rho,pt1,pt2,g,th,m,vposo,gam,2,0)
       w2 = w*sin(alpha)
      pinft = pinft - (w1 + w2)*dz/2.
      end do

c     Calculate pert. potential at center of bottom sfc.

      dz=0.2
      pinfb=0.
      do i=1,49
       x=co(m/4,1)
       z1=-10.+(co(m/4,2)-0.001) + dz*float(i)
      call xzvel(u,w,x,z1,rho,pt1,pt2,g,th,m,vposo,gam,2,0)
       w1 = w*sin(alpha)
       z2=-10.+(co(m/4,2)-0.001) + dz*float(i+1)
      call xzvel(u,w,x,z2,rho,pt1,pt2,g,th,m,vposo,gam,2,0)
       w2 = w*sin(alpha)
      pinfb = pinfb + (w1 + w2)*dz/2.
      end do

c     Top right quarter total potential

      pot(3*m/4,2) = pinft + co(3*m/4,1)*sin(alpha)*cos(rho)
     &  + co(3*m/4,2)*sin(alpha)*sin(rho)
      do i=3*m/4,m-1
      dx = co(i+1,1)-co(i,1)
      dz = co(i+1,2)-co(i,2)
      dli = sqrt(dx**2 + dz**2)
      pot(i+1,2) = pot(i,2) + dli*(velt(i+1)-velt(i))/2.
```

```
      end do

c  Top left quarter total potential

      do i=3*m/4,m/2+2,-1
      dx = co(i-1,1)-co(i,1)
      dz = co(i-1,2)-co(i,2)
      dli = sqrt(dx**2 + dz**2)
      pot(i-1,2) = pot(i,2) - dli*(velt(i-1)-velt(i))/2.
      end do

c  Bottom right quarter total potential

      pot(m/4,2) = pinfb + co(m/4,1)*sin(alpha)*cos(rho)
     & + co(m/4,2)*sin(alpha)*sin(rho)
      do i=m/4,2,-1
      dx = co(i-1,1)-co(i,1)
      dz = co(i-1,2)-co(i,2)
      dli = sqrt(dx**2 + dz**2)
      pot(i-1,2) = pot(i,2) - dli*(velt(i-1)-velt(i))/2.
      end do

c  Bottom Left quarter total potential

      do i=m/4,m/2-1
      dx = co(i+1,1)-co(i,1)
      dz = co(i+1,2)-co(i,2)
      dli = sqrt(dx**2 + dz**2)
      pot(i+1,2) = pot(i,2) + dli*(velt(i+1)-velt(i))/2.
      end do

      do i=1,m
       dpotdt(i) = ( pot(i,2)-pot(i,1) )/dt
       pot(i,1)=pot(i,2)
      if(istep.eq.0)dpotdt(i) = 0.
      end do

c  Calculate Pressure Coefficient and loads

      cm = 0.

      do i=1,m
      phix(i) = ( pot(i,2)
     & - co(i,1)*(velt(i)*cos(th(i))+sin(alpha)*cos(rho))
     & - co(i,2)*(velt(i)*sin(-th(i))+sin(alpha)*sin(rho)) )
     & * tan(eps)

      cp(i) = sin(alpha)**2 - 2.*phix(i)*cos(alpha) - phix(i)**2
     & - velt(i)**2
     & -2.*xc*tan(eps)*phidot(1)*r(i)*
     & ( sin(bet(i))*(velt(i)*cos(th(i))-vn(i)*sin(alpha)*sin(th(i)))
     & - cos(bet(i))*(velt(i)*sin(th(i))+vn(i)*sin(alpha)*cos(th(i))))
     & - 2.*xc*tan(eps)*dpotdt(i)

c  write(8,*)co(i,1),',',co(i,2),',',cp(i)
```

```
      cm = cm + cp(i)*dl(i)*5./48.*( sin(th(i))*co(i,2)
     & + cos(th(i))*co(i,1) )

      end do


c   Motion

      phi(2) = phi(1) + phidot(1)*dt
      rho = pi/2. + phi(2)

      phidot(2) = phidot(1) + ( dens*cm*cr**5*tan(eps)**2
     & /inertia - 0.001*phidot(1)*inrf )*dt

c=====================Forced=============
c   phi(2) =        0.872 * cos(0.5*tstar)
c   phidot(2) = - 0.872 * 0.5* sin(0.5*tstar)
c       rho = pi/2. + phi(2)
c========================================

      dphi = phi(2) - phi(1)

      vpos(1,1)=v11*cos(dphi)-v12*sin(dphi)
      vpos(1,2)=v11*sin(dphi)+v12*cos(dphi)
      vpos(2,1)=v21*cos(dphi)-v22*sin(dphi)
      vpos(2,2)=v21*sin(dphi)+v22*cos(dphi)

      if(mod(istep,10).eq.0)then
      write(8,*)tstar,(phi(1))*180./pi,cm,
     &             deltl*180./pi,deltr*180./pi
      write(9,*)tstar,(phi(1))*180./pi,vposo(1,1),vposo(1,2),
     &             gam(1,3),vposo(2,1),vposo(2,2),gam(2,3)
      write(*,*)istep,(phi(1))*180./pi,cm,deltl*180./pi
     &,deltr*180./pi
      end if

c   Control

      if(istep.ge.icntrl)then

      if(phidot(2).gt.0.)then
        deltr = kgain*phidot(2)
            if (deltr .gt. 70.) deltr=70.
      else
      deltr = 0.
      endif

      if(phidot(2).lt.0.)then
        deltl = kgain*abs(phidot(2))
            if (deltl .gt. 70.) deltl=70.
      else
      deltl = 0.
      endif
```

```fortran
      end if

      phi(1) = phi(2)
      phidot(1) = phidot(2)

      istep = istep + 1
      tstar = istep*dt

      if(istep.lt.iend)goto 5
c         enddo
      close(unit=8)
      close(unit=9)
      stop
      end

c==================================================================

      subroutine matrx(a,n,g)

c     matrx is a matrix reducer of the Gaussian type
c     a(i,j) is the matrix, g(i) is the solution vector

      real a(200,200),temp(200,200),g(200)


c     initialize the g vector to all zeros

      do i=1,n-1
       g(i)=0.
      end do

c     convert coefficient matrix
c     to upper triangular form

      do i=1,n-1
 5    if(abs(a(i,i)).lt.0.0000001)goto 9

      p=a(i,i)
      do j=i,n
       a(i,j)=a(i,j)/p
      end do

      do k=i+1,n-1
       p2=a(k,i)
       do l=i,n
        a(k,l)=a(k,l)-p2*a(i,l)
       end do
      end do
      end do

c     back substitute triangularized matrix to get
c     values of solution vector

      do i=n-1,1,-1
```

```fortran
      g(i)=a(i,n)
      do j=1,n-1
       a(i,i)=0.
       g(i)=g(i)-a(i,j)*g(j)
      end do
     end do

     return

c     order matrix so that diagonal coefficients are
c     not=0 and stop if matrix is singular

  9 if(i.ne.n-1)then
     do j=1,n
      temp(i,j)=a(i,j)
      a(i,j)=a(i+1,j)
      a(i+1,j)=temp(i,j)
     end do
     goto 5
    else
     goto 10
    end if

 10   write(*,*)' NO SOLUTION '

    stop
    end

C===================================================================

    subroutine body(m,ept,deltl,deltr)

c     this subroutine calculates the nodal coordinates
c     of the body surface panels
c ***   NOTE: PANEL 1 @ TE. TOP SFC., NUMBERING SCHEME
c             COUNTER-CLOCKWISE                      ***

    real pi,theta,xc,thick,z,ept(200,2),eptt(200,2)

    pi=4.*atan(1.)

    bevang = 45.*pi/180.
    toc=0.085
    bevx=toc/tan(bevang)

c top surface

    do i=0,m/2
      theta=pi*float(i)/float(m/2)
      xc =  ( 1. + cos(theta) )/2.
    z = 0.
    ept(i+1,1)=xc
    ept(i+1,2)=z + toc
    end do
```

```
c   bottom surface

    do i=1,m/2
     theta=pi*float(i)/float(m/2)+pi
     xc = (1. + cos(theta) )/2.

    if(xc.ge.1.-bevx)then
      z=-(1.-xc)*tan(bevang)
    else
      if(xc.le.bevx)then
        z=-xc*tan(bevang)
      else
        z=-toc
      end if
    end if

    ept(m/2+i+1,1)=xc
    ept(m/2+i+1,2)=z + toc

    end do

    do i=1,m+1
     eptt(i,1)=ept(i,1)
     eptt(i,2)=ept(i,2)
    end do

    do i=1,m+1

    if(eptt(i,1).ge.1.-bevx)then
    ept(i,1)=(1.-bevx)+(eptt(i,1)-1.+bevx)*cos(deltr)
      & +(eptt(i,2))*sin(deltr)
    ept(i,2)=-(eptt(i,1)-1.+bevx)*sin(deltr)
      & +(eptt(i,2))*cos(deltr)
    end if

    if(eptt(i,1).le.bevx)then
    ept(i,1)=bevx - (bevx-eptt(i,1))*cos(deltl)
      & -(eptt(i,2))*sin(deltl)
    ept(i,2)=-(bevx-eptt(i,1))*sin(deltl)
      & +(eptt(i,2))*cos(deltl)
    end if

    ept(i,1) = 2.*(ept(i,1)-0.5)
    ept(i,2)=ept(i,2)-toc/2

    end do

    return
    end

C===============================================================

    subroutine xzvel(u,w,x,z,rho,pt1,pt2,g,th,m,vposo,gam,nv,nf)

    real pi,x,z,rho,g(200),th(200),vposo(2,2),pt1(200,2)
```

```
      real pt2(200,2),gam(2,3),cox

      pi=4.*atan(1.)

c  wing influence

      uwing=0.
      wwing=0.

      do j=1,m

      xt=x-pt1(j,1)
      zt=z-pt1(j,2)
      x2t=pt2(j,1)-pt1(j,1)
      z2t=pt2(j,2)-pt1(j,2)
      cox=(pt2(j,1)-pt1(j,1))/2.+pt1(j,1)

      xl=xt*cos(th(j))+zt*sin(th(j))
      zl=-xt*sin(th(j))+zt*cos(th(j))
      x2l=x2t*cos(th(j))+z2t*sin(th(j))
      z2l=0.

      r1=sqrt(xl**2+zl**2)
      r2=sqrt( (xl-x2l)**2+zl**2 )
      th1=atan2(zl,xl)
      th2=atan2(zl,xl-x2l)

      uls= 1./(2.*pi)*log(r1/r2)
          ulv= 1./(2.*pi)*(th2-th1)
      wls= 1./(2.*pi)*(th2-th1)
          wlv= 1./(2.*pi)*log(r2/r1)

      uwing = uwing +  (uls*g(j) + ulv*g(m+1) )*cos(-th(j))
     &  +( wls*g(j) + wlv*g(m+1) )*sin(-th(j))
      wwing = wwing + (-uls*g(j) - ulv*g(m+1) )*sin(-th(j))
     &  +( wls*g(j) + wlv*g(m+1) )*cos(-th(j))

      end do

c  freestream influence

      if(nf.eq.1)then
       uinf = cos(rho)
       winf = sin(rho)
      else
       uinf = 0.
       winf = 0.
      end if

c  vortex influence

      uvort = 0.
      wvort = 0.

      do i=1,nv
```

```
xv=vposo(i,1)
zv=vposo(i,2)
  rcore=sqrt((x-xv)**2+(z-zv)**2)
if(rcore.lt.0.005)then
 uvt=0.
 wvt=0.
else
 uvt=gam(i,3)/(2.*pi)*( (z-zv)/( (x-xv)**2 + (z-zv)**2 ) )
 wvt=-gam(i,3)/(2.*pi)*( (x-xv)/( (x-xv)**2 + (z-zv)**2 ) )
end if

uvort = uvort + uvt
wvort = wvort + wvt

end do

u = uwing + uinf + uvort
w = wwing + winf + wvort
return
end
```

VITA

Steven Roberts

Candidate for the Degree of

Master of Science

Thesis: A MODEL FOR EVALUATING CONTROL OF UNSTEADY LEADING
EDGE VORTEX FLOWS

Major Field: Mechanical Engineering

Biographical:

Education: Graduated from Fairview High School, Fairview, Oklahoma in May
1987; received Bachelor of Science degree in Mechanical Engineering with
an Aerospace Option from Oklahoma State University, Stillwater,
Oklahoma in May 1992. Completed the requirements for the Master of
Science degree with a major in Mechanical Engineering at Oklahoma State
University in July, 1997.

Experience: Employed by Oklahoma State University, Department of Mechanical
Engineering as an undergraduate and as a graduate research assistant;
Oklahoma State University, Department of Mechanical Engineering, 1988
to 1994; Employed by Fluid Technologies, Incorporated, Stillwater,
Oklahoma as a design engineer; 1995; Employed by FlightSafety
International as a propulsion design engineer, 1995 to present.

Professional Memberships: American Institute of Aeronautics and Astronautics,
American Society of Mechanical Engineers, National Society of
Professional Engineers, Oklahoma Society of Professional Engineers